bioRxiv preprint doi: https://doi.org/10.1101/2021.08.30.458235; this version posted August 31, 2021. The copyright holder for this preprint (which was not certified by peer review) is the author/funder, who has granted bioRxiv a license to display the preprint in perpetuity. It is made available under aCC-BY-NC-ND 4.0 International license.

R-loop homeostasis and cancer mutagenesis promoted by the DNA cytosine deaminase APOBEC3B

Jennifer L. McCann[1-4,#], Agnese Cristini[5,#], Emily K. Law[1-4,##], Seo Yun Lee[6,##], Michael Tellier[5], Michael A. Carpenter[1-4], Chiara Beghè[5], Jae Jin Kim[6], Matthew C. Jarvis[2-4], Bojana Stefanovska[2-4], Nuri A. Temiz[2,7], Erik N. Bergstrom[8-10], Daniel J. Salamango[2-4], Margaret R. Brown[2-4], Shona Murphy[5], Ludmil B. Alexandrov[8-10], Kyle M. Miller[6,11], Natalia Gromak[5,*] & Reuben S. Harris[1-4,*]

[1] Howard Hughes Medical Institute, University of Minnesota, Minneapolis, Minnesota, USA, 55455
[2] Masonic Cancer Center, University of Minnesota, Minneapolis, Minnesota, USA, 55455
[3] Institute for Molecular Virology, University of Minnesota, Minneapolis, Minnesota, USA, 55455
[4] Department of Biochemistry, Molecular Biology and Biophysics, University of Minnesota, Minneapolis, Minnesota, USA, 55455
[5] Sir William Dunn School of Pathology, University of Oxford, South Parks Road, Oxford, UK, OX1 3RE
[6] Department of Molecular Biosciences, University of Texas at Austin, Austin, Texas, USA, 78712
[7] Institute for Health Informatics, University of Minnesota, Minneapolis, MN, USA, 55455
[8] Department of Cellular and Molecular Medicine, UC San Diego, La Jolla, California, USA, 92093
[9] Department of Bioengineering, UC San Diego, La Jolla, California, USA, 92093
[10] Moores Cancer Center, UC San Diego, La Jolla, CA, 92037, USA
[11] Livestrong Cancer Institutes, Dell Medical School, University of Texas at Austin, Austin, Texas, USA, 78712
[#] Equal primary contributions; [##] Equal secondary contributions
* Correspondence: natalia.gromak@path.ox.ac.uk and rsh@umn.edu

Running Title: APOBEC3B in R-loop biology and mutagenesis

Manuscript Information: Abstract 149 words; Article including Refs & Legends 60,000 characters; Figs. 1-8; Supplementary Information: Methods; Tables S1-2; Figs. S1-6

bioRxiv preprint doi: https://doi.org/10.1101/2021.08.30.458235; this version posted August 31, 2021. The copyright holder for this preprint (which was not certified by peer review) is the author/funder, who has granted bioRxiv a license to display the preprint in perpetuity. It is made available under aCC-BY-NC-ND 4.0 International license.

Abstract

The single-stranded DNA cytosine-to-uracil deaminase APOBEC3B is an antiviral protein implicated in cancer. However, its substrates in cells are not fully delineated. Here, APOBEC3B proteomics reveal interactions with a surprising number of R-loop factors. Biochemical experiments show APOBEC3B binding to R-loops in human cells and *in vitro*. Genetic experiments demonstrate R-loop increases in cells lacking APOBEC3B and decreases in cells overexpressing APOBEC3B. Genome-wide analyses show major changes in the overall landscape of physiological and stimulus-induced R-loops with thousands of differentially altered regions as well as binding of APOBEC3B to many of these sites. APOBEC3 mutagenesis impacts overexpressed genes and splice factor mutant tumors preferentially, and APOBEC3-attributed *kataegis* are enriched in RTCW consistent with APOBEC3B deamination. Taken together with the fact that APOBEC3B binds single-stranded DNA and RNA and preferentially deaminates DNA, these results support a mechanism in which APOBEC3B mediates R-loop homeostasis and contributes to R-loop mutagenesis in cancer.

Key words

APOBEC mutation signature; APOBEC3B; Cancer mutagenesis; DNA damage; DNA deamination; *Kataegis*; R-loop homeostasis; R-loop mutagenesis; RNA/DNA hybrids

Highlights

* Unbiased proteomics link antiviral APOBEC3B to R-loop regulation

* Systematic alterations of APOBEC3B levels trigger corresponding changes in R-loops

bioRxiv preprint doi: https://doi.org/10.1101/2021.08.30.458235; this version posted August 31, 2021. The copyright holder for this preprint (which was not certified by peer review) is the author/funder, who has granted bioRxiv a license to display the preprint in perpetuity. It is made available under aCC-BY-NC-ND 4.0 International license.

* APOBEC3B binds R-loops in living cells and *in vitro*

* Bioinformatics analyses support an R-loop deamination and mutation model

Introduction

The APOBEC3 family of single-stranded (ss)DNA cytosine deaminases are critical players in the overall innate immune response to viral infection (reviewed by refs.[1,2]). Popularized initially by potent HIV-1 restriction activity[3-6], the seven human APOBEC3 enzymes collectively elicit activity against a broad number of DNA-based viruses including retroviruses (HIV-1, HTLV-1), hepadnaviruses (HBV), papillomaviruses (HPV), parvoviruses (AAV), polyomaviruses (JC and BKPyV), and herpesviruses (EBV, HSV-1) (reviewed by refs.[1,2]). An important biochemical feature of this family of enzymes is an intrinsic preference for different nucleobases immediately 5' of target cytosines[7-11]. For example, APOBEC3B (A3B) and APOBEC3A (A3A) preferentially deaminate cytosines in 5'TC motifs and the related antibody gene diversification enzyme AID targets 5'AC and 5'GC motifs.

In addition to beneficial functions in innate and adaptive immunity, multiple DNA cytosine deaminases have detrimental roles in cancer mutagenesis (reviewed by refs.[1,12-17]). Misprocessing of AID-catalyzed deamination events in antibody gene variable and switch regions can result in DNA breaks and chromosomal translocations in B cell malignancies (reviewed by ref.[17]). Off-target deamination of other genes also occurs at lower frequencies and the resulting mutations may contribute to B cell lineage-derived leukemias and lymphomas[18,19]. In comparison, large-scale tumor sequencing projects have reported an APOBEC mutation signature in a wide variety of cancer types

bioRxiv preprint doi: https://doi.org/10.1101/2021.08.30.458235; this version posted August 31, 2021. The copyright holder for this preprint (which was not certified by peer review) is the author/funder, who has granted bioRxiv a license to display the preprint in perpetuity. It is made available under aCC-BY-NC-ND 4.0 International license.

including those derived from breast, lung, head/neck, cervix, and bladder tissues (see recent pan-cancer analysis[20] and reviews above). In cancer, the APOBEC mutation signature is defined as C-to-T transitions and C-to-G transversions in 5'TCA and 5'TCT motifs to help distinguish from other mutational processes[21-25]. Recent estimates indicate that APOBEC enzymes are the second most prevalent mutation-generating process in human cancer following clock-like mutagenesis which is attributed to ageing[20].

Despite extensive documentation of the APOBEC mutation signature in cancer, the precise molecular mechanisms governing this mutational process are still unclear. One challenge is the possibility that at least two enzymes, A3B and A3A, combine in different ways to generate the overall signature (*e.g.*, refs.[21-23,26-28]). However, a few mechanistic insights have still been inferred from the physical characteristics of genomes with, for instance, APOBEC mutations associating with chromosomal DNA replication and specifically with C-to-U deamination events in the lagging strand template[29-34]. Other genomic features and processes with exposed ssDNA may be similarly prone to APOBEC mutagenesis such as single-stranded loop regions of DNA hairpins[35,36] and ssDNA tracts in recombination and repair reactions, which sometimes manifest clusters of strand-coordinated APOBEC3-attributed mutations (*aka. kataegis*; *e.g.*, refs.[25,35,37]). Together, these studies have indicated a passive diffusion mechanism in which simple expression of A3B and/or A3A leads to random encounters with any exposed ssDNA followed in some instances by processive local deamination.

Another potential substrate for APOBEC enzymes is ssDNA exposed by R-loop formation. R-loops occur when nascent RNA re-anneals to the transcribed DNA strand,

bioRxiv preprint doi: https://doi.org/10.1101/2021.08.30.458235; this version posted August 31, 2021. The copyright holder for this preprint (which was not certified by peer review) is the author/funder, who has granted bioRxiv a license to display the preprint in perpetuity. It is made available under aCC-BY-NC-ND 4.0 International license.

creating a three-stranded structure containing an RNA/DNA hybrid and a displaced non-transcribed ssDNA strand (reviewed by refs.[38-40]). R-loops are critical for the specialized mechanism of AID-catalyzed antibody gene hypermutation and class switch recombination in B lymphocytes (reviewed by refs.[41,42]). R-loops also represent a prominent source of genome instability associated with human disease, including cancer (*e.g.*, refs.[43-45]; reviewed by refs.[39,40,46-51]). However, evidence linking APOBEC enzymes to R-loop-associated mutation and genome instability is presently lacking. A potential clue came from recent studies showing a mismatch repair-dependent synthetic lethal interaction between A3B activity and uracil excision repair disruption[52]. This report suggested that the toxic lesions may represent U/G mispairs, which are unlikely to arise through replication but may be created by transcription-associated processes, such as C-to-U deamination within a R-loop.

A3B is strongly implicated in cancer mutagenesis based on several criteria including nuclear localization, overexpression in tumors, upregulation by cancer-causing viruses such as HPV, and associations with clinical outcomes (reviewed by refs.[1,12-14]). To gain deeper insights into the pathological role of A3B in cancer mutagenesis, an unbiased affinity purification and mass spectrometry (AP-MS) approach was used to identify A3B-interacting proteins. Two dozen proteins were recovered in biologically-independent experiments, and 60% of the resulting high-confidence interactors had been reported previously as R-loop-associated factors in RNA/DNA hybrid AP-MS experiments[53]. A comprehensive series of genetic, cell biology, biochemistry, genomic, and bioinformatic studies was therefore undertaken to investigate the relationship between A3B and R-loops. Surprisingly, the results indicated that A3B functions in R-

bioRxiv preprint doi: https://doi.org/10.1101/2021.08.30.458235; this version posted August 31, 2021. The copyright holder for this preprint (which was not certified by peer review) is the author/funder, who has granted bioRxiv a license to display the preprint in perpetuity. It is made available under aCC-BY-NC-ND 4.0 International license.

loop homeostasis. Moreover, R-loop regions impacted by cellular A3B show significant enrichments for APOBEC3 signature mutations including *kataegis* in breast tumors. Altogether, these results reveal an unanticipated role for A3B in R-loop biology and a distinct mechanism of transcription-associated cancer mutagenesis.

Results

APOBEC3B interacts with R-loops and R-loop-associated proteins

Little is known about the molecular processes that serve to regulate the mutagenic activities of A3B. To address this gap in knowledge, a functional A3B-2xStrep-3xFlag construct (hereafter A3B-SF) was expressed in 293T cells, anti-Strep affinity-purified, and subjected to mass spectrometry to identify interacting proteins (AP-MS workflow schematic in **Fig. S1a**). This procedure included exogenous RNase A and high salt concentrations to enrich for direct and strong interactions, respectively. Immunoblots, Coomassie gels, and DNA deaminase activity assays were used to validate the presence, enrichment, and activity of affinity-purified A3B (**Fig. S1b-d**). Expression of an eGFP-SF construct and an empty 2xStrep-3xFlag vector was analyzed in parallel as negative controls.

Six independent AP-MS experiments yielded a total of 24 specific A3B-interacting proteins (**Table S1**; independent confirmation in **Fig. S1e-f**). These proteins were abundant in all 6 A3B-SF data sets and, importantly, absent in GFP-SF or empty vector datasets. Only CDK4, which regulates A3B localization during the cell cycle[54], and hnRNPUL1, which tethered to Cas9 is capable of targeting A3B for base editing[55],

bioRxiv preprint doi: https://doi.org/10.1101/2021.08.30.458235; this version posted August 31, 2021. The copyright holder for this preprint (which was not certified by peer review) is the author/funder, who has granted bioRxiv a license to display the preprint in perpetuity. It is made available under aCC-BY-NC-ND 4.0 International license.

had been reported previously. However, literature analyses revealed that 60% of these A3B interactors had been found independently in S9.6 AP-MS experiments[53] (**Fig. 1a-b**). As the S9.6 mAb binds strongly to RNA/DNA hybrid structures[56,57], this significant interactome overlap suggested that A3B may also interact with R-loops. To test this hypothesis, interactions between A3B and multiple R-loop factors were confirmed in co-immunoprecipitation (co-IP) experiments. For example, doxycycline (Dox)-inducible A3B-eGFP was immunoprecipitated from MCF10A cells with an anti-eGFP antibody and the R-loop-associated protein hnRNPUL1 was detected by immunoblotting (system validation in **Fig. 1c** and representative co-IP in **Fig. 1d**). Parallel slot blots showed that R-loops also co-purified with A3B-eGFP, and the RNase H sensitivity of the signal demonstrated the specific detection of RNA/DNA hybrids (**Fig. 1d**).

The S9.6 mAb was then used to IP RNA/DNA hybrids from MCF10A cells treated with phorbol 12-myristate 13-acetate (PMA) to induce endogenous *A3B* expression[58]. Immunoblotting confirmed enrichment of an established R-loop interacting protein, TOP1[59,60], and a shared R-loop and A3B interactor, hnRNPUL1, in all S9.6 IP reactions except those saturated with a synthetic RNA/DNA hybrid competitor (**Fig. 1e**). The non-R-loop-interacting protein Lamin B1 served as a negative control for these IP reactions. Endogenous A3B copurified with R-loop structures in basal non-induced conditions and this interaction increased following PMA treatment (**Fig. 1e**). Importantly, no A3B signal was detected in S9.6 pull downs from *A3B*-null MCF10A cells, which demonstrated interaction specificity (**Fig. 1e**; *A3B* knockout construction and validation in **Fig. S2a-d**).

Elevated nuclear R-loop levels in *A3B*-null and *A3B*-depleted cells

bioRxiv preprint doi: https://doi.org/10.1101/2021.08.30.458235; this version posted August 31, 2021. The copyright holder for this preprint (which was not certified by peer review) is the author/funder, who has granted bioRxiv a license to display the preprint in perpetuity. It is made available under aCC-BY-NC-ND 4.0 International license.

To investigate a potential role for A3B in R-loop biology, R-loop levels were quantified in MCF10A and its *A3B*-null derivative. First, nucleoplasmic S9.6 staining intensity was measured by immunofluorescence (IF) confocal microscopy. These experiments revealed a strong increase in nucleoplasmic S9.6 fluorescence in *A3B*-null cells in comparison to parental MCF10A cells (**Fig. 2a-b**). Second, S9.6 dot blot experiments confirmed elevated R-loop levels in the *A3B*-null MCF10A cells in comparison to the parental line (**Fig. 2c-d**). Importantly, in both series of experiments, RNase H treatment eliminated the increase in R-loop signals observed in the absence of endogenous A3B. S9.6 signal detecting nucleolar rRNA is mostly insensitive to RNase H treatment, as reported[61], and is also largely unaffected by A3B.

To address whether the relationship between A3B and R-loop levels may be a general mechanism, analogous S9.6 IF microscopy and dot blot experiments were done using U2OS cells, which express high levels of endogenous A3B[54,62,63]. U2OS cells were transduced with a validated shRNA to stably deplete endogenous *A3B* or a non-targeting control shRNA[22,64] (*A3B* knockdown validation in **Fig. S2e-g**). In these experiments, *A3B* knockdown caused a strong increase in nucleoplasmic S9.6 staining intensity by IF microscopy in comparison to control transduced cells analyzed in parallel (**Fig. 2e-f**). As above, nearly all nucleoplasmic S9.6 staining was ablated by RNase H treatment, indicating that the signal is specific to RNA/DNA hybrids. An increase in RNA/DNA hybrid signal was also obtained in S9.6 dot blot experiments from *A3B*-depleted versus control transduced cells and, again, specificity was confirmed by RNase H treatment (**Fig. 2g-h**). R-loop imbalances are a known source of DNA damage[38-40], and elevated R-loop levels in *A3B*-null MCF10A and *A3B*-depleted U2OS

bioRxiv preprint doi: https://doi.org/10.1101/2021.08.30.458235; this version posted August 31, 2021. The copyright holder for this preprint (which was not certified by peer review) is the author/funder, who has granted bioRxiv a license to display the preprint in perpetuity. It is made available under aCC-BY-NC-ND 4.0 International license.

cells triggered concomitant increases in DNA break formation as evidenced by γ-H2AX staining (**Fig. 2i-l**). However, it is important to note that these elevated levels of R-loops and DNA damage did not alter overall rates of DNA replication (EdU incorporation) or cell cycle progression (**Fig. S2h-k**).

A3B reduces nuclear R-loop levels through a deamination-dependent mechanism

Given results above showing increased R-loop accumulation upon *A3B* loss, we next asked whether A3B overexpression might have the opposite effect and suppress R-loop formation. U2OS cells were transfected with an expression vector for A3B-eGFP or eGFP as a negative control, incubated 24 hrs to allow for protein expression, treated 4 hrs with the Bromodomain and Extra-Terminal (BET) protein family inhibitor JQ1 to enhance R-loop formation[44,65,66], and then analyzed by IF confocal microscopy for S9.6 staining. In comparison to the eGFP control, A3B-eGFP expression caused a significant decrease in the average intensity of nucleoplasmic S9.6 levels (**Fig. 3a-b**). Interestingly, expression of A3A, which is more active than A3B in ssDNA deamination assays[67,68], had no effect suggesting a specific R-loop role for A3B (**Fig. 3a-b**).

The hallmark biochemical activity of A3B is ssDNA C-to-U deamination (*e.g.*, refs.[22,67,68]; reviewed by refs.[13,69,70]). To determine whether deaminase activity is required for reducing nuclear R-loop levels, U2OS cells were transfected with constructs expressing A3B-eGFP or a single amino acid substitution catalytic mutant E255A, which prevents A3B from deprotonating water and creating the hydroxide ion required for C-to-U deamination (reviewed by refs.[13,69,70]). Importantly, wild-type A3B caused a significant reduction in nucleoplasmic R-loop levels as quantified by S9.6 staining and IF

bioRxiv preprint doi: https://doi.org/10.1101/2021.08.30.458235; this version posted August 31, 2021. The copyright holder for this preprint (which was not certified by peer review) is the author/funder, who has granted bioRxiv a license to display the preprint in perpetuity. It is made available under aCC-BY-NC-ND 4.0 International license.

microscopy, whereas the catalytic mutant had a less pronounced effect despite similar expression levels (**Fig. 3c-d** and data not shown). However, because U2OS cells already express high levels of endogenous A3B (above) and APOBEC3 enzymes including A3B are reported to oligomerize[68,71-75], this intermediate phenotype may be due to oligomerization between overexpressed mutant and endogenous A3B.

Therefore, a series of genetic complementation experiments was performed to compare the activities of wild-type A3B and the E255A catalytic mutant in cells lacking endogenous A3B. First, endogenous *A3B* was depleted from U2OS cells as above, which resulted in lower A3B protein and activity levels (**Fig. 3e**). Second, *A3B*-depleted U2OS cells were stably transfected with shRNA-resistant constructs expressing HA-tagged wild-type A3B, A3B-E255A, or an empty vector control (**Fig. 3e**). The wild-type A3B enzyme but not the E255A catalytic mutant restored ssDNA deaminase activity as expected (**Fig. 3e**). Third, R-loop levels were analyzed by S9.6 dot blot assays. Importantly, complementation with wild-type A3B rescued the effect of *A3B* depletion and caused a significant reduction in R-loops (**Fig. 3f-g**). In contrast, cells complemented with similar levels of the catalytic mutant protein, A3B-E255A, showed no significant change in R-loop levels demonstrating a deamination-dependent mechanism.

APOBEC3B-regulated R-loops are transcription-dependent

R-loop formation normally occurs during the process of transcription when a nascent RNA hybridizes with the template DNA strand and displaces the non-template ssDNA behind the elongating RNA polymerase (reviewed by refs.[38,39,76]). To confirm that A3B-

bioRxiv preprint doi: https://doi.org/10.1101/2021.08.30.458235; this version posted August 31, 2021. The copyright holder for this preprint (which was not certified by peer review) is the author/funder, who has granted bioRxiv a license to display the preprint in perpetuity. It is made available under aCC-BY-NC-ND 4.0 International license.

associated R-loops are transcription-dependent, shCtrl and shA3B U2OS cells were treated with the global transcription inhibitor triptolide[77,78] and IF microscopy analyses were used to quantify R-loop levels. As above, *A3B* depletion resulted in an increase in nucleoplasmic R-loop levels, and triptolide abolished this effect (**Fig. 4a-b**). Dot blot analysis of RNA/DNA hybrids yielded similar results (**Fig. 4c-d**). Complementary data were obtained using a different transcription inhibitor, flavopiridol, which specifically inhibits the CDK9 kinase subunit of the positive transcription elongation factor b (P-TEFb) of RNA polymerase II (*i.e.*, flavopiridol inhibits CDK9, blocks transcription elongation, and concomitantly blocks R-loop accumulation[79]) (**Fig. 4c-d**). These results confirmed that A3B-targeted R-loops are indeed transcription-dependent.

APOBEC3B alters the genome-wide distribution of R-loops

The aforementioned IF confocal microscopy and dot blot results suggested a role for A3B in regulating R-loop levels genome-wide. This possibility was investigated using DNA/RNA hybrid IP (DRIP)-seq experiments. In line with previous studies[79-81], DRIP-seq peaks in wild-type (WT) and *A3B* knockout (KO) MCF10A cells were mainly intragenic and distributed between protein-coding, long non-coding RNA, and enhancer RNA genes (**Fig. 5a-b**). As anticipated by these distributions and the transcription dependence above, the vast majority of DRIP-seq positive regions in WT and KO MCF10A cells occurred in expressed genes (**Fig. S3a**).

A global comparison of DRIP-seq peaks between KO and WT MCF10A revealed changes in the overall R-loop landscape with 8,296 peaks ‘increased’, 13,761 peaks ‘decreased’, and 154,036 peaks ‘unchanged’ (red vs blue traces in **Fig. 5c-e**).

bioRxiv preprint doi: https://doi.org/10.1101/2021.08.30.458235; this version posted August 31, 2021. The copyright holder for this preprint (which was not certified by peer review) is the author/funder, who has granted bioRxiv a license to display the preprint in perpetuity. It is made available under aCC-BY-NC-ND 4.0 International license.

Representative individual gene results are shown for *GADD45A* and *PHLDA1*, *HIST1H1B* and *SYT8*, and *HIST1H1E* and *DDX1*, which show increased, decreased, and unchanged R-loop levels, respectively, in KO cells in comparison to WT cells (**Fig. 5f**, **h**, **j**). These DRIP-seq results were confirmed by gene-specific DRIP-qPCR (**Fig. 5g**, **i**, **k**). As above, DRIP-qPCR signals were reduced significantly by RNase H treatment, further confirming R-loop specificity (**Fig. 5g**, **i**, **k**, striped bars). Differential DRIP signals were not due to transcription differences between the KO and WT cell lines (**Fig. S3b**). As expected, negligible DRIP signals were found in non-expressed genes and intergenic loci (*e.g.*, *TFF1* in **Fig. S3c-d**). In addition, similar DRIP results were obtained in a different cell line (*A3B*-depleted HeLa) analyzed by immunoblotting and qPCR (**Fig. S3e-g**).

APOBEC3B accelerates the kinetics of R-loop resolution

Transcriptional activation by different signal transduction pathways is known to trigger large increases in R-loop formation[82,83]. As the datasets above were generated under normal growth conditions, an additional set of experiments was done to address whether A3B may also affect signal transduction-induced R-loops. Therefore, WT and KO MCF10A lines were treated with PMA to induce the protein kinase C (PKC) and non-canonical (nc)NF-κB signal transduction pathways and, as such, activate the transcription of many genes including endogenous *A3B*[58,84].

First, global R-loop distributions were analyzed by DRIP-seq in WT MCF10A following 2 hrs PMA treatment in comparison to a DMSO control treatment (workflow in **Fig. S4a**). As anticipated, PMA caused changes in the overall R-loop landscape with

bioRxiv preprint doi: https://doi.org/10.1101/2021.08.30.458235; this version posted August 31, 2021. The copyright holder for this preprint (which was not certified by peer review) is the author/funder, who has granted bioRxiv a license to display the preprint in perpetuity. It is made available under aCC-BY-NC-ND 4.0 International license.

13,422 peaks increased, 16,432 peaks decreased, and 171,322 unchanged (**Fig. S4b-d**). Many genes such as *JUNB* and *FOS* were induced strongly by PMA treatment and showed significant increases in DRIP signals (**Fig. S4e-f**). Other genes such as *NAXE* and *ARL4D* showed decreases in DRIP signals (**Fig. S4g-h**), whereas the majority such as *GAPDH* and *GEMIN7* showed no changes in R-loop formation (**Fig. S4i-j**).

Second, a parallel set of ChIP-seq experiments was done in MCF10A with Dox-inducible A3B-eGFP (**Fig. 1c**) to assess whether any of these R-loop categories might be bound by this deaminase (workflow in **Fig. S4a**). An epitope-tagged protein was necessary because ChIP-grade antibodies have yet to be developed for endogenous A3B. Interestingly, A3B-eGFP appeared to bind preferentially to genomic DNA regions coincident with DRIP-seq peaks increased in PMA-treated cells in comparison to vehicle control treated cells (ChIP-seq results superimposed over DRIP-seq results in **Fig. S4b**). In contrast, A3B-eGFP ChIP-seq peaks were mainly unperturbed in genomic DNA regions in which R-loop levels decreased or remained unchanged upon PMA treatment (**Fig. S4c-d**). Representative results were confirmed independently by ChIP-qPCR (**Fig. S4k**). Moreover, quantification indicated that 43% of A3B ChIP peaks overlap with R-loops peaks induced by PMA (P = 0.0001, two-tailed binomial test; 54% overlap for ChIP peaks with >5-fold enrichment compared to uninduced Dox^- condition, P = 0.0008). These results combined to indicate that A3B binds preferentially to genomic DNA regions with evidence for R-loop accumulation.

Third, the PMA-inducibility of this system enabled an assessment of the kinetics of R-loop resolution in the presence and absence of A3B. WT and KO cells were treated with PMA or DMSO for 2 and 6 hrs and then analyzed by DRIP-seq (workflow in **Fig.**

bioRxiv preprint doi: https://doi.org/10.1101/2021.08.30.458235; this version posted August 31, 2021. The copyright holder for this preprint (which was not certified by peer review) is the author/funder, who has granted bioRxiv a license to display the preprint in perpetuity. It is made available under aCC-BY-NC-ND 4.0 International license.

313 **6a**). These timepoints were chosen for analysis because transcription induction and R-
314 loop formation are rapid (2 hrs data above) and A3B protein levels are upregulated
315 maximally by 6 hrs post-PMA treatment[58] (**Fig. 6b-c**). For example, *JUNB* and *DUSP1*
316 have R-loop peaks that are strongly induced by PMA at 2 hrs and these return to near-
317 control levels by 6 hrs (**Fig. 6d**). In contrast, R-loop peaks in the same genes remained
318 significantly elevated and/or showed delayed resolution kinetics in KO cells after 6 hrs
319 PMA treatment (**Fig. 6d**). PMA non-responsive genes used as controls did not show R-
320 loop induction or major differences in R-loop levels after 6 hrs PMA treatment (*e.g.*,
321 *GAPDH* and *HSPA8* in **Fig. 6e**). Moreover, independent IF confocal microscopy studies
322 of the kinetics of R-loop resolution following PMA treatment of WT MCF10A cells
323 showed that nucleoplasmic R-loop levels peak at 2 hrs and decline substantially by 6
324 hrs, whereas no decline (even a modest increase) was observed in *A3B* KO cells (**Fig.**
325 **6f-g**). As above, all DRIP-qPCR and nucleoplasmic R-loop signals were sensitive to
326 RNase H treatment indicating specificity (**Fig. 6d-g**). Taken together with the ChIP data
327 above, the results of these PMA time course experiments indicated that nuclear A3B is
328 recruited to PMA-induced R-loops and contributes to their timely resolution.
329
330 **APOBEC3B biochemical activities required for R-loop resolution**
331 To investigate the biochemical activities of A3B in R-loop resolution, wild-type A3B was
332 purified from 293T cells (**Fig. S5a**) and used for nucleic acid binding and DNA
333 deamination experiments (**Fig. 7** and **Fig. S5b-c**). The various nucleic acids used in
334 these biochemical experiments are depicted in **Fig. 7a**. EMSAs indicated that A3B is
335 capable of binding to R-loop structures (novel), to ssDNA and ssRNA (expected[67,68,85]),

bioRxiv preprint doi: https://doi.org/10.1101/2021.08.30.458235; this version posted August 31, 2021. The copyright holder for this preprint (which was not certified by peer review) is the author/funder, who has granted bioRxiv a license to display the preprint in perpetuity. It is made available under aCC-BY-NC-ND 4.0 International license.

and to lesser extents to dsDNA, dsRNA, or RNA/DNA hybrid (also expected[67,68,85]; **Fig. S5b-c**). These native EMSAs were hard to quantify due to accumulation of large protein/nucleic acid complexes in the wells. We therefore reduced the complexity of binding studies by quantifying the release of fluorescently-labeled ssRNA and ssDNA from A3B by incubating with a broad concentration range of otherwise identical unlabeled nucleic acid competitors. These experiments demonstrated that A3B binds strongly and nearly indistinguishably to both ssRNA and ssDNA (**Fig. 7b**).

RNA is an inferred inhibitor of the ssDNA cytosine deaminase activity of A3B based on experiments in which exogenous RNase A treatment is required to detect ssDNA deaminase activity in cancer cell extracts (*e.g.*, refs.[22,58]). We therefore wondered whether the RNA in R-loop structures might inhibit the ssDNA deaminase activity of A3B on the unpaired ssDNA strand. Qualitative single timepoint reactions indicated clear activity on free ssDNA cytosines and potentially reduced activities on ssDNA cytosines in a bubble, short R-loop, and long R-loop structures (**Fig. 7c**). A quantitative time course comparing A3B activity on free ssDNA versus ssDNA in the context of an R-loop structure indicated that the latter substrate is only about 2-fold less preferred (**Fig. 7d**). These data showed that R-loops can be substrates for A3B-catalyzed ssDNA deamination. The 2-fold diminution in activity may be due to ssDNA inaccessibility caused by the relatively short nature of the synthetic R-loop (21 nucleotides) and/or to competition with unpaired ssDNA or ssRNA.

To gain additional mechanistic insights into A3B function in R-loop biology, we analyzed the nucleoplasmic R-loop phenotypes of an A3B mutant defective in nuclear localization (Mut1)[86] and a mutant incapable of binding strongly to nucleic acid (Mut2)[85].

bioRxiv preprint doi: https://doi.org/10.1101/2021.08.30.458235; this version posted August 31, 2021. The copyright holder for this preprint (which was not certified by peer review) is the author/funder, who has granted bioRxiv a license to display the preprint in perpetuity. It is made available under aCC-BY-NC-ND 4.0 International license.

Both of these activities are governed by the N-terminal domain (NTD) of A3B, and are independent of the C-terminal domain (CTD) that binds much more weakly to ssDNA and catalyzes deamination[67,85,86]. We confirmed the nuclear localization defect of the Mut1 and, interestingly, showed that Mut2 still retains this hallmark activity (**Fig. 7e**). Mut2 was also purified and, in contrast to the wild-type enzyme, confirmed defective in binding to ssRNA and ssDNA using EMSAs (**Fig. S5a** and **Fig. 7f**). However, Mut2 still retained high levels of ssDNA deaminase activity and was similarly active on free ssDNA and short R-loop ssDNA (**Fig. 7g**). This result is consistent with the possibility that unannealed nucleic acid may interfere with the deaminase activity of the WT enzyme (above) but not with Mut2, which has reduced nucleic acid binding activity. Most importantly, in contrast to WT A3B, neither mutant was capable of decreasing nucleoplasmic R-loop levels following JQ1 treatment (**Fig. 7h**). The separation-of-function Mut2 protein also had a diminished capacity to co-IP interactors (**Fig. S1f**). These results indicated that both nuclear localization and nucleic acid binding activities are required for A3B to alter nucleoplasmic R-loop levels.

Genome-wide associations between APOBEC3 signature mutations, gene overexpression, and splicing defects

The involvement of A3B in transcription-dependent R-loop biology led us next to evaluate whether transcribed genes may be preferred sites of mutagenesis. Specifically, we propose a working model in which exposed ssDNA cytosines in R-loop regions are deaminated by A3B and resolved into mutagenic or non-mutagenic outcomes (**Fig. 8a** and **Discussion**). Non-mutagenic outcomes are likely to comprise most resolution

bioRxiv preprint doi: https://doi.org/10.1101/2021.08.30.458235; this version posted August 31, 2021. The copyright holder for this preprint (which was not certified by peer review) is the author/funder, who has granted bioRxiv a license to display the preprint in perpetuity. It is made available under aCC-BY-NC-ND 4.0 International license.

382 events, but these leave no genomic scars and, thus, are invisible to bioinformatics
383 analyses. However, mutagenic R-loop resolution outcomes are predicted to reflect the
384 intrinsic structural preference of A3B for deamination of cytosines in TC motifs[7,87,88] and
385 more broadly in TCW and RTCW extended motifs as defined experimentally and
386 computationally[23,26]. For comparison, A3A elicits a preference for YTCW[23,26,89].

387 One prediction of this model is that a positive association may exist between
388 transcription levels and APOBEC3-attributed mutations. Because previous studies
389 established a correlation between gene expression and R-loop formation[79], we
390 predicted that higher rates of transcription should, at least at some loci, lead to higher
391 rates of R-loop formation and increased exposure to A3B. This idea was addressed
392 using whole-exome sequenced (WES) breast cancers and corresponding RNA-seq data
393 from TCGA project as well as whole-genome sequenced (WGS) breast cancers from
394 the ICGC consortium and normal breast tissue gene expression data from the GTEx
395 project (Methods). An initial association between gene expression levels and
396 APOBEC3-attributed mutations was intriguing but became insignificant after accounting
397 for gene size (**Fig. S6a-b**). However, a strong positive association emerged between
398 the magnitude of gene overexpression in breast cancer compared to normal breast
399 tissue and the proportion of mutations attributable to APOBEC3 deamination (all TCW
400 mutations in **Fig. 8b**, $P < 1.0 \times 10^{-12}$ by student's t-test; RTCW/YTCW breakdown in **Fig.**
401 **S6c**). These analyses indicated that the higher the degree of gene overexpression in
402 breast cancer the higher the proportion of mutations attributable to APOBEC3, with the
403 highest overexpressed gene group showing an average of over 50-fold more APOBEC3
404 signature mutations than any of the three lowest expressed gene groups.

bioRxiv preprint doi: https://doi.org/10.1101/2021.08.30.458235; this version posted August 31, 2021. The copyright holder for this preprint (which was not certified by peer review) is the author/funder, who has granted bioRxiv a license to display the preprint in perpetuity. It is made available under aCC-BY-NC-ND 4.0 International license.

Second, because splicing defects lead to increases in R-loop formation[90-92], our working model predicts that splice factor mutant tumors may manifest elevated levels of APOBEC3 signature mutations. This idea was investigated by splitting the TCGA breast cancer WES data set into tumors with and without mutations in splice factor genes and evaluating associations with the proportion of mutations attributable to APOBEC3 activity. Remarkably, 53% of the breast tumors with mutant splice factor genes (43/81) had significant levels of APOBEC3 signature mutations (**Fig. 8c**). In contrast, only 35% of breast tumors without mutations in the same splice factor gene set (326/841) showed a detectable APOBEC3 mutation signature (**Fig. 8c**; $P < 0.017$ by Fisher's exact test). APOBEC3-attributed mutations in both groups were partitioned into RTCW/YTCW tetranucleotide motifs and, interestingly, the A3B-associated RTCW motif was only absent from one of the splice factor mutant tumors (1/43) in comparison to a significant proportion of the non-splice factor mutant group (52/326) (**Fig. S6d-e**; $P = 0.028$ by Fisher's exact test). Splice factor mutant tumors also had a higher mean percentage of APOBEC3-attributed mutations (39% vs 31%, respectively; $P = 0.042$ by unpaired two-sample Welsh's t-test) as well as higher total numbers of mutations on average than non-splice factor mutated samples ($P = 0.0018$ by Welch's two sample t-test). Even the top quartile of tumors with the strongest APOBEC3 signature had higher total numbers of mutations in the splice factor mutant group ($P = 0.0095$ by Welch's two sample t-test). These relationships between splice factor defects, higher mutation loads, and APOBEC3 mutation signature are not likely due to chance because no other similarly sized gene set selected randomly from housekeeping genes (100,000 random gene set selections) is similarly mutated in TCGA breast cancer data sets (*i.e.*, the observed

bioRxiv preprint doi: https://doi.org/10.1101/2021.08.30.458235; this version posted August 31, 2021. The copyright holder for this preprint (which was not certified by peer review) is the author/funder, who has granted bioRxiv a license to display the preprint in perpetuity. It is made available under aCC-BY-NC-ND 4.0 International license.

splice factor defects are not due to higher rates of mutation; rather, the observed splice factor defects are likely to contribute to the higher rates of mutation). We also noted that APOBEC3-attributed mutations accumulate preferentially on the non-transcribed strand (NTS) over the transcribed strand (TS) in both splice factor mutant and non-mutant tumor groups with a statistical difference that may relate to the underlying mechanism (P = 0.0284 and P = 4.3 x 10^{-12}, respectively, by student's t-test). In further support of a connection between aberrant splicing, R-loop formation, and APOBEC3 mutagenesis, A3B overexpression suppresses the increase in R-loop formation caused by treating U2OS cells with the splicing inhibitor pladienolide B (Plad B; **Fig. 8d**).

Third, because APOBEC3 signature *kataegic* events are undoubtedly due to strand-coordinated deamination by at least one APOBEC3 enzyme[20,25], we asked what proportion of these events occur in genes and, moreover, occur on the NTS versus the TS to potentially reveal which part of the genome may be more susceptible. This analysis focused again on breast cancer due to the large size and overall high quality of the WGS data sets. A global mapping of all *kataegis* events in primary breast adenocarcinomas from the Pan-Cancer Analysis of Whole Genomes (PCAWG) revealed a bimodal distribution with one peak located within 1 kbp of a structural variation breakpoint (SV) and another similarly sized peak much further away from the nearest SV (~1 Mbp; n = 198 WGS data sets; blue bars in **Fig. 8e**). As expected[93], the SV-proximal subset of *kataegis* events is likely due to deamination of resected ssDNA ends during recombination repair. Also expected, non-clustered (*i.e.*, dispersed) APOBEC3-attributed mutations occur on average of >1 Mbp apart (yellow bars in **Fig. 8e**). In contrast, the majority of APOBEC3-attributed *kataegic* events (>75%) map >10

bioRxiv preprint doi: https://doi.org/10.1101/2021.08.30.458235; this version posted August 31, 2021. The copyright holder for this preprint (which was not certified by peer review) is the author/funder, who has granted bioRxiv a license to display the preprint in perpetuity. It is made available under aCC-BY-NC-ND 4.0 International license.

kbp away from SVs and are unlikely to be due to a DNA double-stranded break and recombination-associated mechanism (red bars in **Fig. 8e**). Moreover, a significant proportion of these distal APOBEC3 signature *kataegic* events occur within R-loop regions defined above in DRIP-seq experiments.

To investigate the source of APOBEC3 signature *kataegis*, we plotted overall enrichments for A3B-associated RTCA and A3A-associated YTCA tetranucleotide motifs (R=A or G; Y=C or T)[26] and shaded data points red to distinguish breast tumors with at least one R-loop associated *kataegic* event. This analysis indicated, first, that tumors with APOBEC3 signature *kataegis* are common and, second, that APOBEC3 *kataegic* mutations overlapping R-loop regions, in contrast to dispersed APOBEC3 mutations, are skewed toward RTCA motifs (**Fig. 8f-g**; *Q*-values in each dot plot determined using Mann-Whitney U-tests). Third, the overall RTCW skew of *kataegic* ($\geq$3 mutations per cluster) versus dispersed APOBEC3 mutations was greatest for mutations occurring on the NTS but still evident on the TS and intergenic regions (**Fig. 8f**; P = 0.0006, P = 0.0086, and P = 0.096 respectively, by Fisher's exact tests after FDR correction). For greater stringency, this latter analysis was repeated for longer APOBEC3 *kataegic* tracts ($\geq$5 mutations per cluster) and a statistically significant enrichment was only evident for RTCA events on the NTS of genes [**Fig. 8g**; P = 0.0001 (NTS), P = 0.15 (TS), and P = 0.072 (intergenic)]. Representative NTS *kataegic* events are shown for *PRKCA* and *LGR5* (**Fig. 8h**). Taken together, these different bioinformatic analyses support a model in which at least a subset of R-loop structures is susceptible to C-to-U deamination events most likely catalyzed by A3B.

bioRxiv preprint doi: https://doi.org/10.1101/2021.08.30.458235; this version posted August 31, 2021. The copyright holder for this preprint (which was not certified by peer review) is the author/funder, who has granted bioRxiv a license to display the preprint in perpetuity. It is made available under aCC-BY-NC-ND 4.0 International license.

Discussion

Our studies are the first to report the cellular interactome of A3B and reveal an unanticipated role for this antiviral enzyme in R-loop biology. We delineate a functional relationship between A3B and R-loops with higher R-loop levels occurring upon A3B knockout/down and lower R-loop levels upon A3B overexpression. Genome-wide DRIP-seq experiments in physiological conditions and upon activation of a signal transduction pathway indicated that thousands of R-loops in cells are affected by A3B (*i.e.*, increased or decreased in *A3B*-null cells). This number represents over 10% of R-loops genome-wide, which is comparable to the proportions of R-loops affected by other R-loop regulatory factors, such as TOP1, DDX5, XRN2, and PRMT5[80,94]. These findings are also in line with knowledge that multiple proteins contribute to R-loop regulation, including RNase H1, TOP1, SETX, AQR, UAP56/DDX39B, FANCD2, and BRCA1/2[38,45,80,94-103]. Determining the precise combination of molecular mechanisms responsible for the regulation of a given R-loop remains a challenge for future studies.

In addition to discovering an unanticipated role for A3B in R-loop homeostasis, our studies also shed light on the underlying molecular mechanism of R-loop resolution. First, complementation experiments showed that the mechanism is deaminase-dependent with expression of a single amino acid catalytic mutant (E255A) failing to decrease nucleoplasmic R-loop levels. Second, the nuclear localization activity of A3B is essential. This requirement may seem obvious but is important to help rule-out potential indirect effects such as A3B binding to cytoplasmic factors and affecting their import into the nuclear compartment and participation in R-loop formation. Third, A3B is capable of binding to R-loop structures, and the strong nucleic acid binding activity of

bioRxiv preprint doi: https://doi.org/10.1101/2021.08.30.458235; this version posted August 31, 2021. The copyright holder for this preprint (which was not certified by peer review) is the author/funder, who has granted bioRxiv a license to display the preprint in perpetuity. It is made available under aCC-BY-NC-ND 4.0 International license.

A3B is required for suppressing nucleoplasmic R-loop levels. Our biochemical competition experiments indicated that ssRNA and ssDNA binding activities are comparable in strength. Together with the fact that A3B's strong nucleic acid binding activity resides within the N-terminal half of the protein and the weaker ssDNA binding activity required for catalysis is governed by the C-terminal half of the enzyme, we favor a working model in which direct binding of A3B to nascent ssRNA adjacent to R-loops and/or to ssDNA exposed in R-loop structures is critical for R-loop regulation (**Fig. 8a**). The next steps in such a mechanism may be deamination of exposed ssDNA cytosines in R-loop structures, uracil excision by UNG2, ssDNA breakage by APEX, and recruitment of additional downstream repair factors for resolution, by analogy to the resolution of AID-catalyzed R-loop associated deamination events in immunoglobulin gene switch regions[41,42] and APOBEC-catalyzed editing of R-loop DNA cytosines exposed in Cas9-mediated base editing reactions[104]. Additional tests of this model should consider complications from synthetic lethal interactions such as between A3B overexpression and UNG2 inhibition[52]. Moreover, the relationship between R-loop homeostasis and DNA repair is likely to be complex, and it is easy to imagine how perturbing R-loop levels in either direction (up or down) could lead to elevated DNA damage responses (*e.g.*, γ-H2AX accumulation), as observed here with A3B-deficient cells and elsewhere with other factors[80,95,96,99,105,106]. Notably, forced overexpression of A3B can also cause elevated DNA damage responses including γ-H2AX accumulation[22,52,107].

This proposed mechanism is likely to lead to predominately error-free resolution, which cannot be detected by bioinformatic genomic analyses. However, a subset of the

bioRxiv preprint doi: https://doi.org/10.1101/2021.08.30.458235; this version posted August 31, 2021. The copyright holder for this preprint (which was not certified by peer review) is the author/funder, who has granted bioRxiv a license to display the preprint in perpetuity. It is made available under aCC-BY-NC-ND 4.0 International license.

uracil lesions and/or abasic sites may lead to APOBEC3 signature mutations and, if clustered, to APOBEC3 *kataegic* events. The possibility of such mutagenic outcomes is supported by a dose-responsive association between genes overexpressed in breast cancers compared to normal breast tissue and the proportions of somatic mutations attributed to APOBEC3 deamination (**Fig. 8b**). Moreover, a preferential accumulation of APOBEC3-attributed mutations is also observed in splice factor mutant breast tumors (**Fig. 8c**). As transcription and splicing are interconnected processes[108] and splice factor defects are known to increase R-loop levels[90-92,109], it is easy to imagine how perturbations in these processes may contribute to increased R-loop formation and exposures of single-stranded cytosines to APOBEC3 deaminase activity. This possibility is further supported by recent bioinformatic studies indicating higher APOBEC3 mutation densities on the NTS of actively expressed genes (including the overexpressed genes analyzed here) in multiple cancer types[110]. We cannot exclude the possibility that other APOBEC3 enzymes, most notably A3A, may also be able to contribute to R-loop mutation. However, this alternative is disfavored because A3A overexpression does not affect R-loop levels and, importantly, the majority of APOBEC3 *kataegic* events are observed far away from sites of structural variation and are enriched for mutations in A3B-associated 5'-RTCW motifs (**Fig. 8e-h**).

In addition, because a proportion of APOBEC3 mutagenesis is likely due to deamination of lagging-strand templates during DNA replication[29-31,33,34,94], it is important to emphasize that APOBEC3-catalyzed C-to-U lesions in transcription-associated R-loop structures are likely to attract different subsets of DNA repair enzymes. A uracil in the DNA replication template strand will instruct the proper

bioRxiv preprint doi: https://doi.org/10.1101/2021.08.30.458235; this version posted August 31, 2021. The copyright holder for this preprint (which was not certified by peer review) is the author/funder, who has granted bioRxiv a license to display the preprint in perpetuity. It is made available under aCC-BY-NC-ND 4.0 International license.

543 insertion of an adenine in the nascent strand, which leaves a U:A base pair for UNG2
544 recognition and faithful uracil base excision repair with the net result being a C-to-T
545 transition. A uracil in an R-loop, following R-loop resolution, will lead to a U/G mispair,
546 which may similarly template the insertion of an adenine through replication but can also
547 attract mismatch repair enzymes, which could promote the creation of a longer ssDNA
548 tract and additional APOBEC3 mutagenesis. This possibility is supported by recent
549 results showing a mismatch repair-dependent synthetic lethal interaction between A3B
550 activity and uracil excision repair disruption[52] and a role for mismatch repair in the
551 creation of *omikli* (shorter-than-*kataegic* tracts of APOBEC3-attributed mutations)[111]. It
552 is also supported by precedents with AID-dependent antibody gene diversification in B
553 lymphocytes where both uracil base excision repair and mismatch repair have integral
554 roles[41,42]. Of course, uracil lesions in both DNA replication template strands and R-loops
555 can lead to alternative outcomes including uracil excision, abasic site bypass or
556 cleavage, single- and double-stranded DNA breaks, and larger-scale genetic
557 aberrations including translocations. A3B-mediated mutagenesis may be particularly
558 relevant in cancer cells that display both increased A3B expression and R-loop
559 dysregulation resulting from mutations in splice factors or other R-loop regulatory
560 factors (*e.g.*, BRCA1/2 and Fanconi anemia proteins[99,100,102,112,113]) and/or activation of
561 signal transduction pathway-induced transcriptional programs[82,83] such as during
562 conditions of oncogenic signaling, infection, or inflammation[58,114,115]. Therefore, in
563 addition to archetypic base substitution mutations, it is tempting to speculate that at
564 least some R-loop-associated DNA damage and chromosome aberrations (reviewed by
565 refs.[39,46,48,116]) may be instigated by the A3B-dependent mechanism described here.

bioRxiv preprint doi: https://doi.org/10.1101/2021.08.30.458235; this version posted August 31, 2021. The copyright holder for this preprint (which was not certified by peer review) is the author/funder, who has granted bioRxiv a license to display the preprint in perpetuity. It is made available under aCC-BY-NC-ND 4.0 International license.

In addition to the resolution mechanism discussed above, a potentially overlapping alternative is A3B-dependent recruitment of other proteins known to promote R-loop resolution. Such interactions could be direct or bridged, for instance, by RNA or ssDNA. In support of this possibility, the A3B separation-of-function mutant Mut2, which is deficient in nucleic acid binding but proficient in nuclear import and DNA deamination, is less capable of interacting with several R-loop associated factors (Fig. S1f). Moreover, although our studies here focused on AP-MS interactions specific to A3B (absent from all controls), a number of A3B-enriched factors (present at lower levels in at least one control reaction), such as the helicase DHX9, might be worthy of future investigation. This DNA/RNA helicase was reported recently as a suppressor of the antiviral activity of A3B[117]. It is harder to envisage a mechanism to explain the subset of genes that elicit decreased R-loop levels in the absence of A3B. In these instances, A3B may be blocking a known resolution activity, such as a helicase that loads via RNA or ssDNA, from gaining access to R-loops. Further studies on A3B regulation of R-loop homeostasis will undoubtedly be exciting as answers will shed additional light on R-loop biology, provide insights into the normal physiological functions of A3B in innate antiviral immune responses, and may help define additional targetable nodes in A3B-overexpressing tumor types such as breast cancer.

Acknowledgements

We thank N.J. Proudfoot for critically reading the manuscript, J. Becker and J. Duda for corroborative localization data with A3B mutants, the University of Minnesota Imaging Center for access to instrumentation, and the Oxford Genomics Centre at the Wellcome

bioRxiv preprint doi: https://doi.org/10.1101/2021.08.30.458235; this version posted August 31, 2021. The copyright holder for this preprint (which was not certified by peer review) is the author/funder, who has granted bioRxiv a license to display the preprint in perpetuity. It is made available under aCC-BY-NC-ND 4.0 International license.

589 Centre for Human Genetics (funded by Wellcome Trust grant 203141/Z/16/Z) for the
590 generation and initial processing of the sequencing data. This work was supported by
591 NCI P01 CA234228 (to RSH), NIAID R37 AI064046 (to RSH), and by the University of
592 Minnesota Masonic Cancer Center, Academic Health Center, and College of Biological
593 Sciences. NG lab is supported by the Royal Society University Research fellowship
594 (BVD07340), Royal Society Enhancement Award (RGF\EA\180023) and EPA Research
595 Fund (Sir William Dunn School of Pathology, University of Oxford) to NG and CRUK
596 development fund (CRUK DF-0119) to AC and NG. MT and SM are supported by the
597 Wellcome Trust Investigator Award to SM (WT210641/Z/18/Z). KMM lab was supported
598 by NCI RO1 CA198279 and NCI RO1 CA201268. LBA lab was supported by US NIH
599 R01 ES030993 and R01 ES032547. Salary support for JLM was provided initially by an
600 NSF Graduate Research Fellowship (Grant Number 00039202) and subsequently by
601 HHMI. Salary support for MCJ was provided in part by T32 CA009138 and
602 subsequently NCI F31 CA243306. Salary support for BS was provided by HHMI with
603 some supplies provided by the Ovarian Cancer Research Alliance (Ann and Sol
604 Schreiber Mentored Investigator Award 812337). Salary support for DJS was provided
605 by NIAID K99 AI147811. RSH is the Margaret Harvey Schering Land Grant Chair for
606 Cancer Research, a Distinguished University McKnight Professor, and an Investigator
607 of the Howard Hughes Medical Institute.

608

609 ## Author contributions

610 R.S.H., J.L.M., A.C. and N.G. conceived and designed these studies. J.L.M. and A.C.
611 performed experiments unless otherwise noted. E.K.L. generated U2OS knockdown

bioRxiv preprint doi: https://doi.org/10.1101/2021.08.30.458235; this version posted August 31, 2021. The copyright holder for this preprint (which was not certified by peer review) is the author/funder, who has granted bioRxiv a license to display the preprint in perpetuity. It is made available under aCC-BY-NC-ND 4.0 International license.

and complement cell lines along with assisted in tissue culture and genomic DNA isolations for dot blot experiments. S.L., J.K. and K.M.M. performed and quantified IF data. M.T. and S.M. conducted DRIP-seq and ChIP-seq data analysis. C.B. performed DRIP-qPCR validations and HeLa R-loop IP. B.S. assisted with cell culture experiments and R-loop quantification. M.R.B. assisted with cell culture studies. M.C.J., N.A.T., D.J.S., E.N.B. and L.B.A. performed bioinformatic analyses. M.A.C. contributed biochemical experiments. R.S.H. and J.L.M. drafted the manuscript with input from all other authors.

Competing interest statement

The authors have no conflicts to declare.

References

1. Green, A.M. & Weitzman, M.D. The spectrum of APOBEC3 activity: from anti-viral agents to anti-cancer opportunities. *DNA Repair (Amst)* **83**, 102700 (2019).
2. Harris, R.S. & Dudley, J.P. APOBECs and virus restriction. *Virology* **479-480**, 131-45 (2015).
3. Sheehy, A.M., Gaddis, N.C., Choi, J.D. & Malim, M.H. Isolation of a human gene that inhibits HIV-1 infection and is suppressed by the viral Vif protein. *Nature* **418**, 646-50 (2002).
4. Harris, R.S. *et al.* DNA deamination mediates innate immunity to retroviral infection. *Cell* **113**, 803-9 (2003).

bioRxiv preprint doi: https://doi.org/10.1101/2021.08.30.458235; this version posted August 31, 2021. The copyright holder for this preprint (which was not certified by peer review) is the author/funder, who has granted bioRxiv a license to display the preprint in perpetuity. It is made available under aCC-BY-NC-ND 4.0 International license.

5. Zhang, H. *et al.* The cytidine deaminase CEM15 induces hypermutation in newly synthesized HIV-1 DNA. *Nature* **424**, 94-8 (2003).

6. Mangeat, B. *et al.* Broad antiretroviral defence by human APOBEC3G through lethal editing of nascent reverse transcripts. *Nature* **424**, 99-103 (2003).

7. Shi, K. *et al.* Structural basis for targeted DNA cytosine deamination and mutagenesis by APOBEC3A and APOBEC3B. *Nat Struct Mol Biol* **24**, 131-139 (2017).

8. Kohli, R.M. *et al.* Local sequence targeting in the AID/APOBEC family differentially impacts retroviral restriction and antibody diversification. *J Biol Chem* **285**, 40956-64 (2010).

9. Rathore, A. *et al.* The local dinucleotide preference of APOBEC3G can be altered from 5'-CC to 5'-TC by a single amino acid substitution. *J Mol Biol* **425**, 4442-54 (2013).

10. Wang, M., Rada, C. & Neuberger, M.S. Altering the spectrum of immunoglobulin V gene somatic hypermutation by modifying the active site of AID. *J Exp Med* **207**, 141-53 (2010).

11. Carpenter, M.A., Rajagurubandara, E., Wijesinghe, P. & Bhagwat, A.S. Determinants of sequence-specificity within human AID and APOBEC3G. *DNA Repair (Amst)* **9**, 579-87 (2010).

12. Swanton, C., McGranahan, N., Starrett, G.J. & Harris, R.S. APOBEC enzymes: mutagenic fuel for cancer evolution and heterogeneity. *Cancer Discov* **5**, 704-12 (2015).

bioRxiv preprint doi: https://doi.org/10.1101/2021.08.30.458235; this version posted August 31, 2021. The copyright holder for this preprint (which was not certified by peer review) is the author/funder, who has granted bioRxiv a license to display the preprint in perpetuity. It is made available under aCC-BY-NC-ND 4.0 International license.

13. Siriwardena, S.U., Chen, K. & Bhagwat, A.S. Functions and malfunctions of mammalian DNA-cytosine deaminases. *Chem Rev* **116**, 12688-12710 (2016).

14. Venkatesan, S. *et al.* Perspective: APOBEC mutagenesis in drug resistance and immune escape in HIV and cancer evolution. *Ann Oncol* **29**, 563-572 (2018).

15. Roberts, S.A. & Gordenin, D.A. Hypermutation in human cancer genomes: footprints and mechanisms. *Nat Rev Cancer* **14**, 786-800 (2014).

16. Helleday, T., Eshtad, S. & Nik-Zainal, S. Mechanisms underlying mutational signatures in human cancers. *Nat Rev Genet* **15**, 585-98 (2014).

17. Casellas, R. *et al.* Mutations, kataegis and translocations in B cells: understanding AID promiscuous activity. *Nat Rev Immunol* **16**, 164-76 (2016).

18. Basso, K. & Dalla-Favera, R. Germinal centres and B cell lymphomagenesis. *Nat Rev Immunol* **15**, 172-84 (2015).

19. Liu, M. *et al.* Two levels of protection for the B cell genome during somatic hypermutation. *Nature* **451**, 841-5 (2008).

20. Alexandrov, L.B. *et al.* The repertoire of mutational signatures in human cancer. *Nature* **578**, 94-101 (2020).

21. Burns, M.B., Temiz, N.A. & Harris, R.S. Evidence for APOBEC3B mutagenesis in multiple human cancers. *Nat Genet* **45**, 977-83 (2013).

22. Burns, M.B. *et al.* APOBEC3B is an enzymatic source of mutation in breast cancer. *Nature* **494**, 366-70 (2013).

23. Roberts, S.A. *et al.* An APOBEC cytidine deaminase mutagenesis pattern is widespread in human cancers. *Nat Genet* **45**, 970-6 (2013).

bioRxiv preprint doi: https://doi.org/10.1101/2021.08.30.458235; this version posted August 31, 2021. The copyright holder for this preprint (which was not certified by peer review) is the author/funder, who has granted bioRxiv a license to display the preprint in perpetuity. It is made available under aCC-BY-NC-ND 4.0 International license.

678 24. Alexandrov, L.B. *et al.* Signatures of mutational processes in human cancer. *Nature*
679 **500**, 415-21 (2013).
680 25. Nik-Zainal, S. *et al.* Mutational processes molding the genomes of 21 breast
681 cancers. *Cell* **149**, 979-93 (2012).
682 26. Chan, K. *et al.* An APOBEC3A hypermutation signature is distinguishable from the
683 signature of background mutagenesis by APOBEC3B in human cancers. *Nat*
684 *Genet* **47**, 1067-72 (2015).
685 27. Nik-Zainal, S. *et al.* Association of a germline copy number polymorphism of
686 APOBEC3A and APOBEC3B with burden of putative APOBEC-dependent
687 mutations in breast cancer. *Nat Genet* **46**, 487-91 (2014).
688 28. Cortez, L.M. *et al.* APOBEC3A is a prominent cytidine deaminase in breast cancer.
689 *PLoS Genet* **15**, e1008545 (2019).
690 29. Seplyarskiy, V.B. *et al.* APOBEC-induced mutations in human cancers are strongly
691 enriched on the lagging DNA strand during replication. *Genome Res* **26**, 174-82
692 (2016).
693 30. Hoopes, J.I. *et al.* APOBEC3A and APOBEC3B preferentially deaminates the
694 lagging strand template during DNA replication. *Cell Rep* **14**, 1273-1282 (2016).
695 31. Bhagwat, A.S. *et al.* Strand-biased cytosine deamination at the replication fork
696 causes cytosine to thymine mutations in *Escherichia coli*. *Proc Natl Acad Sci U S*
697 *A* **113**, 2176-81 (2016).
698 32. Haradhvala, N.J. *et al.* Mutational strand asymmetries in cancer genomes reveal
699 mechanisms of DNA damage and repair. *Cell* **164**, 538-49 (2016).

bioRxiv preprint doi: https://doi.org/10.1101/2021.08.30.458235; this version posted August 31, 2021. The copyright holder for this preprint (which was not certified by peer review) is the author/funder, who has granted bioRxiv a license to display the preprint in perpetuity. It is made available under aCC-BY-NC-ND 4.0 International license.

33. Morganella, S. *et al.* The topography of mutational processes in breast cancer genomes. *Nat Commun* **7**, 11383 (2016).

34. Sui, Y. *et al.* Analysis of APOBEC-induced mutations in yeast strains with low levels of replicative DNA polymerases. *Proc Natl Acad Sci U S A* **117**, 9440-9450 (2020).

35. Nik-Zainal, S. *et al.* Landscape of somatic mutations in 560 breast cancer whole-genome sequences. *Nature* **534**, 47-54 (2016).

36. Buisson, R. *et al.* Passenger hotspot mutations in cancer driven by APOBEC3A and mesoscale genomic features. *Science* **364**(2019).

37. Taylor, B.J. *et al.* DNA deaminases induce break-associated mutation showers with implication of APOBEC3B and 3A in breast cancer kataegis. *Elife* **2**, e00534 (2013).

38. García-Muse, T. & Aguilera, A. R Loops: from physiological to pathological roles. *Cell* **179**, 604-618 (2019).

39. Crossley, M.P., Bocek, M. & Cimprich, K.A. R-Loops as cellular regulators and genomic threats. *Mol Cell* **73**, 398-411 (2019).

40. Belotserkovskii, B.P., Tornaletti, S., D'Souza, A.D. & Hanawalt, P.C. R-loop generation during transcription: Formation, processing and cellular outcomes. *DNA Repair (Amst)* **71**, 69-81 (2018).

41. Zanotti, K.J. & Gearhart, P.J. Antibody diversification caused by disrupted mismatch repair and promiscuous DNA polymerases. *DNA Repair (Amst)* **38**, 110-116 (2016).

bioRxiv preprint doi: https://doi.org/10.1101/2021.08.30.458235; this version posted August 31, 2021. The copyright holder for this preprint (which was not certified by peer review) is the author/funder, who has granted bioRxiv a license to display the preprint in perpetuity. It is made available under aCC-BY-NC-ND 4.0 International license.

722 42. Pilzecker, B. & Jacobs, H. Mutating for good: DNA damage responses during
723 somatic hypermutation. *Front Immunol* **10**, 438 (2019).
724 43. Hamperl, S., Bocek, M.J., Saldivar, J.C., Swigut, T. & Cimprich, K.A. Transcription-
725 replication conflict orientation modulates R-Loop levels and activates distinct
726 DNA damage responses. *Cell* **170**, 774-786.e19 (2017).
727 44. Kim, J.J. *et al.* Systematic bromodomain protein screens identify homologous
728 recombination and R-loop suppression pathways involved in genome integrity.
729 *Genes Dev* **33**, 1751-1774 (2019).
730 45. Bayona-Feliu, A., Barroso, S., Muñoz, S. & Aguilera, A. The SWI/SNF chromatin
731 remodeling complex helps resolve R-loop-mediated transcription-replication
732 conflicts. *Nat Genet* **53**, 1050-1063 (2021).
733 46. Sollier, J. & Cimprich, K.A. Breaking bad: R-loops and genome integrity. *Trends Cell*
734 *Biol* **25**, 514-22 (2015).
735 47. Aguilera, A. & García-Muse, T. R loops: from transcription byproducts to threats to
736 genome stability. *Mol Cell* **46**, 115-24 (2012).
737 48. Skourti-Stathaki, K. & Proudfoot, N.J. A double-edged sword: R loops as threats to
738 genome integrity and powerful regulators of gene expression. *Genes Dev* **28**,
739 1384-96 (2014).
740 49. Richard, P. & Manley, J.L. R Loops and links to human disease. *J Mol Biol* **429**,
741 3168-3180 (2017).
742 50. Groh, M. & Gromak, N. Out of balance: R-loops in human disease. *PLoS Genet* **10**,
743 e1004630 (2014).

bioRxiv preprint doi: https://doi.org/10.1101/2021.08.30.458235; this version posted August 31, 2021. The copyright holder for this preprint (which was not certified by peer review) is the author/funder, who has granted bioRxiv a license to display the preprint in perpetuity. It is made available under aCC-BY-NC-ND 4.0 International license.

744 51. Wells, J.P., White, J. & Stirling, P.C. R Loops and their composite cancer
745 connections. *Trends Cancer* **5**, 619-631 (2019).
746 52. Serebrenik, A.A. *et al.* The deaminase APOBEC3B triggers the death of cells
747 lacking uracil DNA glycosylase. *Proc Natl Acad Sci U S A* **116**, 22158-22163
748 (2019).
749 53. Cristini, A., Groh, M., Kristiansen, M.S. & Gromak, N. RNA/DNA hybrid interactome
750 identifies DXH9 as a molecular player in transcriptional termination and R-Loop-
751 associated DNA damage. *Cell Rep* **23**, 1891-1905 (2018).
752 54. McCann, J.L. *et al.* The DNA deaminase APOBEC3B interacts with the cell-cycle
753 protein CDK4 and disrupts CDK4-mediated nuclear import of Cyclin D1. *J Biol*
754 *Chem* **294**, 12099-12111 (2019).
755 55. McCann, J.L., Salamango, D.J., Law, E.K., Brown, W.L. & Harris, R.S. MagnEdit-
756 interacting factors that recruit DNA-editing enzymes to single base targets. *Life*
757 *Sci Alliance* **3**, e201900606 (2020).
758 56. Boguslawski, S.J. *et al.* Characterization of monoclonal antibody to DNA.RNA and
759 its application to immunodetection of hybrids. *J Immunol Methods* **89**, 123-30
760 (1986).
761 57. Phillips, D.D. *et al.* The sub-nanomolar binding of DNA-RNA hybrids by the single-
762 chain Fv fragment of antibody S9.6. *J Mol Recognit* **26**, 376-81 (2013).
763 58. Leonard, B. *et al.* The PKC/NF-κB signaling pathway induces APOBEC3B
764 expression in multiple human cancers. *Cancer Res* **75**, 4538-47 (2015).

bioRxiv preprint doi: https://doi.org/10.1101/2021.08.30.458235; this version posted August 31, 2021. The copyright holder for this preprint (which was not certified by peer review) is the author/funder, who has granted bioRxiv a license to display the preprint in perpetuity. It is made available under aCC-BY-NC-ND 4.0 International license.

765 59. El Hage, A., French, S.L., Beyer, A.L. & Tollervey, D. Loss of Topoisomerase I leads
766 to R-loop-mediated transcriptional blocks during ribosomal RNA synthesis.
767 *Genes Dev* **24**, 1546-58 (2010).
768 60. Tuduri, S. *et al.* Topoisomerase I suppresses genomic instability by preventing
769 interference between replication and transcription. *Nat Cell Biol* **11**, 1315-24
770 (2009).
771 61. Smolka, J.A., Sanz, L.A., Hartono, S.R. & Chédin, F. Recognition of RNA by the
772 S9.6 antibody creates pervasive artifacts when imaging RNA:DNA hybrids. *J Cell*
773 *Biol* **220**, e202004079 (2021).
774 62. Cheng, A.Z. *et al.* Epstein-Barr virus BORF2 inhibits cellular APOBEC3B to
775 preserve viral genome integrity. *Nat Microbiol* **4**, 78-88 (2019).
776 63. Jarvis, M.C., Ebrahimi, D., Temiz, N.A. & Harris, R.S. Mutation signatures including
777 APOBEC in cancer cell lines. *JNCI Cancer Spectr* **2**, pky002 (2018).
778 64. Leonard, B. *et al.* APOBEC3B upregulation and genomic mutation patterns in
779 serous ovarian carcinoma. *Cancer Res* **73**, 7222-31 (2013).
780 65. Edwards, D.S. *et al.* BRD4 prevents R-Loop formation and transcription-replication
781 conflicts by ensuring efficient transcription elongation. *Cell Rep* **32**, 108166
782 (2020).
783 66. Lam, F.C. *et al.* BRD4 prevents the accumulation of R-loops and protects against
784 transcription-replication collision events and DNA damage. *Nat Commun* **11**,
785 4083 (2020).

bioRxiv preprint doi: https://doi.org/10.1101/2021.08.30.458235; this version posted August 31, 2021. The copyright holder for this preprint (which was not certified by peer review) is the author/funder, who has granted bioRxiv a license to display the preprint in perpetuity. It is made available under aCC-BY-NC-ND 4.0 International license.

786 67. Ito, F., Fu, Y., Kao, S.A., Yang, H. & Chen, X.S. Family-wide comparative analysis
787 of cytidine and methylcytidine deamination by eleven human APOBEC proteins.
788 *J Mol Biol* **429**, 1787-1799 (2017).
789 68. Adolph, M.B., Love, R.P., Feng, Y. & Chelico, L. Enzyme cycling contributes to
790 efficient induction of genome mutagenesis by the cytidine deaminase
791 APOBEC3B. *Nucleic Acids Res* **45**, 11925-11940 (2017).
792 69. DeNizio, J.E., Schutsky, E.K., Berrios, K.N., Liu, M.Y. & Kohli, R.M. Harnessing
793 natural DNA modifying activities for editing of the genome and epigenome. *Curr*
794 *Opin Chem Biol* **45**, 10-17 (2018).
795 70. Olson, M.E., Harris, R.S. & Harki, D.A. APOBEC enzymes as targets for virus and
796 cancer therapy. *Cell Chem Biol* **25**, 36-49 (2018).
797 71. Chaurasiya, K.R. *et al.* Oligomerization transforms human APOBEC3G from an
798 efficient enzyme to a slowly dissociating nucleic acid-binding protein. *Nat Chem*
799 **6**, 28-33 (2014).
800 72. Ara, A., Love, R.P. & Chelico, L. Different mutagenic potential of HIV-1 restriction
801 factors APOBEC3G and APOBEC3F is determined by distinct single-stranded
802 DNA scanning mechanisms. *PLoS Pathog* **10**, e1004024 (2014).
803 73. Chelico, L., Prochnow, C., Erie, D.A., Chen, X.S. & Goodman, M.F. Structural model
804 for deoxycytidine deamination mechanisms of the HIV-1 inactivation enzyme
805 APOBEC3G. *J Biol Chem* **285**, 16195-205 (2010).
806 74. Bennett, R.P., Salter, J.D., Liu, X., Wedekind, J.E. & Smith, H.C. APOBEC3G
807 subunits self-associate via the C-terminal deaminase domain. *J Biol Chem* **283**,
808 33329-36 (2008).

bioRxiv preprint doi: https://doi.org/10.1101/2021.08.30.458235; this version posted August 31, 2021. The copyright holder for this preprint (which was not certified by peer review) is the author/funder, who has granted bioRxiv a license to display the preprint in perpetuity. It is made available under aCC-BY-NC-ND 4.0 International license.

809 75. Li, J. *et al.* APOBEC3 multimerization correlates with HIV-1 packaging and
810 restriction activity in living cells. *J Mol Biol* **426**, 1296-307 (2014).
811 76. Allison, D.F. & Wang, G.G. R-loops: formation, function, and relevance to cell
812 stress. *Cell Stress* **3**, 38-46 (2019).
813 77. Bensaude, O. Inhibiting eukaryotic transcription: Which compound to choose? How
814 to evaluate its activity? *Transcription* **2**, 103-108 (2011).
815 78. Wang, Y., Lu, J.J., He, L. & Yu, Q. Triptolide (TPL) inhibits global transcription by
816 inducing proteasome-dependent degradation of RNA polymerase II (Pol II). *PLoS*
817 *One* **6**, e23993 (2011).
818 79. Sanz, L.A. *et al.* Prevalent, dynamic, and conserved R-Loop structures associate
819 with specific epigenomic signatures in mammals. *Mol Cell* **63**, 167-78 (2016).
820 80. Manzo, S.G. *et al.* DNA Topoisomerase I differentially modulates R-loops across the
821 human genome. *Genome Biol* **19**, 100 (2018).
822 81. Nojima, T. *et al.* Deregulated expression of mammalian lncRNA through loss of
823 SPT6 induces R-Loop formation, replication stress, and cellular senescence. *Mol*
824 *Cell* **72**, 970-984.e7 (2018).
825 82. Kotsantis, P. *et al.* Increased global transcription activity as a mechanism of
826 replication stress in cancer. *Nat Commun* **7**, 13087 (2016).
827 83. Stork, C.T. *et al.* Co-transcriptional R-loops are the main cause of estrogen-induced
828 DNA damage. *Elife* **5**, e17548 (2016).
829 84. Holden, N.S. *et al.* Phorbol ester-stimulated NF-κB-dependent transcription: roles for
830 isoforms of novel protein kinase C. *Cell Signal* **20**, 1338-48 (2008).

bioRxiv preprint doi: https://doi.org/10.1101/2021.08.30.458235; this version posted August 31, 2021. The copyright holder for this preprint (which was not certified by peer review) is the author/funder, who has granted bioRxiv a license to display the preprint in perpetuity. It is made available under aCC-BY-NC-ND 4.0 International license.

831 85. Xiao, X. *et al.* Structural determinants of APOBEC3B non-catalytic domain for
832 molecular assembly and catalytic regulation. *Nucleic Acids Res* **45**, 7540 (2017).
833 86. Salamango, D.J. *et al.* APOBEC3B nuclear localization requires two distinct N-
834 terminal domain surfaces. *J Mol Biol* **430**, 2695-2708 (2018).
835 87. Hou, S. *et al.* Structural Analysis of the Active Site and DNA Binding of Human
836 Cytidine Deaminase APOBEC3B. *J Chem Theory Comput* **15**, 637-647 (2019).
837 88. Shi, K. *et al.* Active site plasticity and possible modes of chemical inhibition of the
838 human DNA deaminase APOBEC3B. *FASEB Bioadv* **2**, 49-58 (2020).
839 89. Law, E.K. *et al.* APOBEC3A catalyzes mutation and drives carcinogenesis in vivo. *J*
840 *Exp Med* **217**(2020).
841 90. Li, X. & Manley, J.L. Inactivation of the SR protein splicing factor ASF/SF2 results in
842 genomic instability. *Cell* **122**, 365-78 (2005).
843 91. Chen, L. *et al.* The augmented R-Loop is a unifying mechanism for myelodysplastic
844 syndromes induced by high-risk splicing factor mutations. *Mol Cell* **69**, 412-
845 425.e6 (2018).
846 92. Wan, Y. *et al.* Splicing function of mitotic regulators links R-loop-mediated DNA
847 damage to tumor cell killing. *J Cell Biol* **209**, 235-46 (2015).
848 93. ICGC/TCGA. Pan-cancer analysis of whole genomes. *Nature* **578**, 82-93 (2020).
849 94. Villarreal, O.D., Mersaoui, S.Y., Yu, Z., Masson, J.Y. & Richard, S. Genome-wide R-
850 loop analysis defines unique roles for DDX5, XRN2, and PRMT5 in DNA/RNA
851 hybrid resolution. *Life Sci Alliance* **3**, e202000762 (2020).

bioRxiv preprint doi: https://doi.org/10.1101/2021.08.30.458235; this version posted August 31, 2021. The copyright holder for this preprint (which was not certified by peer review) is the author/funder, who has granted bioRxiv a license to display the preprint in perpetuity. It is made available under aCC-BY-NC-ND 4.0 International license.

852 95. Pérez-Calero, C. *et al.* UAP56/DDX39B is a major cotranscriptional RNA-DNA
853 helicase that unwinds harmful R loops genome-wide. *Genes Dev* **34**, 898-912
854 (2020).
855 96. Cohen, S. *et al.* Senataxin resolves RNA:DNA hybrids forming at DNA double-
856 strand breaks to prevent translocations. *Nat Commun* **9**, 533 (2018).
857 97. Skourti-Stathaki, K., Proudfoot, N.J. & Gromak, N. Human senataxin resolves
858 RNA/DNA hybrids formed at transcriptional pause sites to promote Xrn2-
859 dependent termination. *Mol Cell* **42**, 794-805 (2011).
860 98. Sollier, J. *et al.* Transcription-coupled nucleotide excision repair factors promote R-
861 loop-induced genome instability. *Mol Cell* **56**, 777-85 (2014).
862 99. Bhatia, V. *et al.* BRCA2 prevents R-loop accumulation and associates with TREX-2
863 mRNA export factor PCID2. *Nature* **511**, 362-5 (2014).
864 100. Shivji, M.K.K., Renaudin, X., Williams, Ç. & Venkitaraman, A.R. BRCA2 regulates
865 transcription elongation by RNA Polymerase II to prevent R-Loop accumulation.
866 *Cell Rep* **22**, 1031-1039 (2018).
867 101. Chen, L. *et al.* R-ChIP using inactive RNase H reveals dynamic coupling of R-
868 loops with transcriptional pausing at gene promoters. *Mol Cell* **68**, 745-757.e5
869 (2017).
870 102. Hatchi, E. *et al.* BRCA1 recruitment to transcriptional pause sites is required for R-
871 loop-driven DNA damage repair. *Mol Cell* **57**, 636-647 (2015).
872 103. Liang, Z. *et al.* Binding of FANCI-FANCD2 complex to RNA and R-Loops
873 stimulates robust FANCD2 monoubiquitination. *Cell Rep* **26**, 564-572.e5 (2019).

bioRxiv preprint doi: https://doi.org/10.1101/2021.08.30.458235; this version posted August 31, 2021. The copyright holder for this preprint (which was not certified by peer review) is the author/funder, who has granted bioRxiv a license to display the preprint in perpetuity. It is made available under aCC-BY-NC-ND 4.0 International license.

874 104. Gu, S., Bodai, Z., Cowan, Q.T. & Komor, A.C. Base editors: Expanding the types
875 of DNA damage products harnessed for genome editing. *Gene Genome Ed*
876 **1**(2021).
877 105. Morales, J.C. *et al.* XRN2 links transcription termination to DNA damage and
878 replication stress. *PLoS Genet* **12**, e1006107 (2016).
879 106. Mersaoui, S.Y. *et al.* Arginine methylation of the DDX5 helicase RGG/RG motif by
880 PRMT5 regulates resolution of RNA:DNA hybrids. *EMBO J* **38**, e100986 (2019).
881 107. Nikkila, J. *et al.* Elevated APOBEC3B expression drives a kataegic-like mutation
882 signature and replication stress-related therapeutic vulnerabilities in p53-
883 defective cells. *Br J Cancer* **117**, 113-123 (2017).
884 108. Tellier, M., Maudlin, I. & Murphy, S. Transcription and splicing: A two-way street.
885 *Wiley Interdiscip Rev RNA* **11**, e1593 (2020).
886 109. Zhang, J. *et al.* Disease-causing mutations in SF3B1 alter splicing by disrupting
887 interaction with SUGP1. *Mol Cell* **76**, 82-95.e7 (2019).
888 110. Chervova, A. *et al.* Analysis of gene expression and mutation data points on
889 contribution of transcription to the mutagenesis by APOBEC enzymes. *NAR*
890 *Cancer* **3**, zcab025 (2021).
891 111. Mas-Ponte, D. & Supek, F. DNA mismatch repair promotes APOBEC3-mediated
892 diffuse hypermutation in human cancers. *Nat Genet* **52**, 958-968 (2020).
893 112. García-Rubio, M.L. *et al.* The Fanconi anemia pathway protects genome integrity
894 from R-loops. *PLoS Genet* **11**, e1005674 (2015).
895 113. Schwab, R.A. *et al.* The Fanconi anemia pathway maintains genome stability by
896 coordinating replication and transcription. *Mol Cell* **60**, 351-61 (2015).

bioRxiv preprint doi: https://doi.org/10.1101/2021.08.30.458235; this version posted August 31, 2021. The copyright holder for this preprint (which was not certified by peer review) is the author/funder, who has granted bioRxiv a license to display the preprint in perpetuity. It is made available under aCC-BY-NC-ND 4.0 International license.

114. Periyasamy, M. *et al.* Induction of APOBEC3B expression by chemotherapy drugs is mediated by DNA-PK-directed activation of NF-κB. *Oncogene* **40**, 1077-1090 (2021).

115. Roelofs, P.A. *et al.* Characterization of the mechanism by which the RB/E2F pathway controls expression of the cancer genomic DNA deaminase APOBEC3B. *Elife* **9**(2020).

116. Hamperl, S. & Cimprich, K.A. The contribution of co-transcriptional RNA:DNA hybrid structures to DNA damage and genome instability. *DNA Repair (Amst)* **19**, 84-94 (2014).

117. Chen, Y. *et al.* DHX9 interacts with APOBEC3B and attenuates the anti-HBV effect of APOBEC3B. *Emerg Microbes Infect* **9**, 366-377 (2020).

bioRxiv preprint doi: https://doi.org/10.1101/2021.08.30.458235; this version posted August 31, 2021. The copyright holder for this preprint (which was not certified by peer review) is the author/funder, who has granted bioRxiv a license to display the preprint in perpetuity. It is made available under aCC-BY-NC-ND 4.0 International license.

Figure legends

Fig. 1. A3B interacts with R-loop-associated proteins

a, Information on shared proteins between A3B and S9.6 AP-MS datasets.

b, Pie chart depicting overlap between A3B and S9.6 AP-MS datasets.

c, Immunoblot and IF microscopy analysis of MCF10A-TREx-A3B-eGFP cells treated with vehicle or Dox (1 μg/mL, 24 hrs). Nuclear A3B-eGFP is green and nuclear DNA is blue (DAPI; representative images; 10 μm scale bar).

d, Immunoblots of A3B-eGFP or IgG IP from TREx-A3B-eGFP MCF10A cells +/- Dox (1 μg/ml, 24 hrs), treated with PMA (25 ng/ml, 2 hrs), and probed with indicated antibodies (upper images). Slot blot of A3B-eGFP IP from TREx-A3B-eGFP MCF10A cells +/- Dox (1 μg/ml, 24 hrs) probed with S9.6 antibody (lower images). RNase H (RNH) treatment confirmed specificity of R-loop signal.

e, Immunoblots of the indicated proteins in input lysates and S9.6 IP reactions from MCF10A (WT) or *A3B*-null derivatives (KO) treated with PMA (25 ng/ml, 5 hrs). R-loop specificity is indicated by signal depletion by RNA/DNA hybrid competitor.

Fig. 2. Elevated nuclear R-loop levels in *A3B*-null and *A3B*-depleted cells

a-b, IF images and quantification of MCF10A (WT) and *A3B*-null (KO) cells stained with S9.6 (green) and DAPI (blue). Diminution of nucleoplasmic S9.6 signal by exogenous RNase H (RNH) confirmed signal specificity (representative images; 5 μm scale bar; n > 100 nuclei per condition; red bars represent mean ± SEM; ****, $P < 0.0001$ by Mann-

bioRxiv preprint doi: https://doi.org/10.1101/2021.08.30.458235; this version posted August 31, 2021. The copyright holder for this preprint (which was not certified by peer review) is the author/funder, who has granted bioRxiv a license to display the preprint in perpetuity. It is made available under aCC-BY-NC-ND 4.0 International license.

Whitney test).

c-d, S9.6 dot blot analysis of a MCF10A (WT) and *A3B*-null (KO) genomic DNA dilution series +/- exogenous RNase H (RNH; representative images). Parallel dsDNA dot blots provided a loading control. Quantification normalized to the most concentrated WT signal (n ≥ 4; mean ± SEM; *, $P < 0.05$ by two-tailed unpaired t-test).

e-f, IF images and quantification of U2OS shCtrl and shA3B cells stained with S9.6 (green) and DAPI (blue). Diminution of nucleoplasmic S9.6 signal by exogenous RNase H (RNH) confirmed signal specificity (representative images; 5 μm scale bar; n > 100 nuclei per condition; red bars represent mean ± SEM; ****, $P < 0.0001$ by Mann-Whitney test).

g-h, S9.6 dot blot analysis of a U2OS shCtrl and shA3B genomic DNA dilution series +/- exogenous RNase H (RNH; representative images). Parallel dsDNA dot blots provided a loading control. Quantification normalized to the most concentrated shCtrl signal (n ≥ 4; mean ± SEM; ***, $P < 0.001$ by two-tailed unpaired t-test).

i-j, IF images and quantification of MCF10A (WT) and *A3B*-null (KO) cells stained with S9.6 (green), DAPI (blue), and γ-H2AX (representative images; 5 μm scale bar; n > 100 nuclei per condition; red bars represent mean ± SEM; ****, $P < 0.0001$ by Mann-Whitney test, ***, $P < 0.001$ by two-tailed unpaired t-test).

k-l, IF images and quantification of U2OS shCtrl and shA3B cells stained with S9.6 (green), DAPI (blue), and γ-H2AX (representative images; 5 μm scale bar; n > 100 nuclei per condition; red bars represent mean ± SEM; ****, $P < 0.0001$ by Mann-Whitney test, ***, $P < 0.001$ by two-tailed unpaired t-test).

bioRxiv preprint doi: https://doi.org/10.1101/2021.08.30.458235; this version posted August 31, 2021. The copyright holder for this preprint (which was not certified by peer review) is the author/funder, who has granted bioRxiv a license to display the preprint in perpetuity. It is made available under aCC-BY-NC-ND 4.0 International license.

Fig. 3. A3B overexpression reduces nuclear R-loop levels

a-d, IF images (a and c) and quantification (b and d) of U2OS cells expressing the denoted eGFP construct (green) and stained with S9.6 (red) and DAPI (blue). Upper panel shows experimental workflow and lower panel representative images (5 μm scale bar; n > 60 nuclei per condition; red bars represent mean ± SEM; *, $P < 0.05$ and ***, $P < 0.001$ by one-way ANOVA; ns, not significant).

e, Immunoblots of U2OS shCtrl or shA3B cells complemented with empty vector (EV), A3B-HA, or A3B-E255A-HA. The lower image shows the results of a DNA deaminase activity assay with extracts from the indicated cell lines (reaction quantification below with purified A3A as a positive control and reaction buffer as a negative control).

f-g, Dot blot analysis of U2OS shCtrl or shA3B cells complemented with empty vector (EV), A3B-HA, or A3B-E255A-HA. A genomic DNA dilution series +/- exogenous RNase H (RNH) was probed with either S9.6 antibody or dsDNA antibody as a loading control (representative images). Quantification normalized to the most concentrated shCtrl signal (n = 3; mean ± SEM; *, $P < 0.05$ by two-tailed unpaired t-test; ns, not significant).

Fig. 4. A3B-regulated R-loops are transcription-dependent

a-b, IF images and quantification of U2OS shCtrl and shA3B cells treated with triptolide (1 μM, 4 hrs) and subsequently stained with S9.6 (green) and DAPI (blue; representative images; 5 μm scale bar; n > 130 nuclei per condition; red bars represent mean ± SEM; ***, $P < 0.001$ and ****, $P < 0.0001$ by one-way ANOVA; ns, not significant).

c-d, S9.6 dot blot analysis of a genomic DNA dilution series +/- RNH from U2OS shCtrl

bioRxiv preprint doi: https://doi.org/10.1101/2021.08.30.458235; this version posted August 31, 2021. The copyright holder for this preprint (which was not certified by peer review) is the author/funder, who has granted bioRxiv a license to display the preprint in perpetuity. It is made available under aCC-BY-NC-ND 4.0 International license.

or shA3B cells treated with triptolide (TRP; 1 μM, 4 hrs) or flavopiridol (FLV; 1 μM, 1 hr; representative images). Parallel dsDNA dot blots provided a loading control. Quantification was normalized to the most concentrated shCtrl/DMSO signal (n = 3; mean ± SEM; *, $P < 0.05$; **, $P < 0.01$ by two-tailed unpaired t-test).

Fig. 5. A3B affects a large proportion of R-loops genome-wide

a-b, Pie graphs representing R-loop distributions in wild-type (WT) and *A3B*-null (KO) MCF10A cells.

c-e, Meta-analysis of read density (FPKM) for DRIP-seq results from wild-type (WT, blue) and *A3B*-null MCF10A (KO, red) partitioned into 3 groups (increased, decreased, and unchanged) as described in the text. Input read densities are indicated by overlapping gray lines.

f-g, **h-i**, **j-k**, DRIP-seq profiles for representative genes in each of the groups defined in panel c-e. Independent quantification by DRIP-qPCR -/+ RNase H (RNH) treatment (striped bars) is shown in the histogram to the right (n ≥ 4; means ± SEM expressed as percentage of input; *, $P < 0.05$; **, $P < 0.01$; ****, $P < 0.0001$ by two-tailed unpaired t-test; ns, not significant).

Fig. 6. Kinetics of R-loop induction and resolution

a, Schematic of the DRIP-seq workflow used for panels d-e.

b, RT-qPCR of *A3B* mRNA from MCF10A (WT) and *A3B*-null (KO) cells treated with PMA (25 ng/ml) for the indicated times. Values are expressed relative to the housekeeping gene, *TBP* (n = 3; mean ± SEM; knockout levels not detectable).

bioRxiv preprint doi: https://doi.org/10.1101/2021.08.30.458235; this version posted August 31, 2021. The copyright holder for this preprint (which was not certified by peer review) is the author/funder, who has granted bioRxiv a license to display the preprint in perpetuity. It is made available under aCC-BY-NC-ND 4.0 International license.

c, Immunoblots of extracts from MCF10A (WT) and *A3B*-null (KO) cells treated with PMA (25 ng/ml) for the indicated times and probed with indicated antibodies.

d, DRIP-seq profiles for two PMA-responsive genes, *JUNB* and *DUSP1*, in DMSO or PMA-treated MCF10A (WT; upper profiles) and *A3B*-null (KO; lower profiles). Independent quantification by DRIP-qPCR -/+ RNase H (RNH) treatment (striped bars) is shown in the histogram to the right (n ≥ 4; mean ± SEM normalized to DMSO WT; *, $P < 0.05$ and **, $P < 0.01$ by two-tailed unpaired t-test).

e, DRIP-seq profiles for two PMA non-responsive genes, *GAPDH* and *HSPA8*, in DMSO or PMA-treated MCF10A (WT; upper profiles) and *A3B*-null (KO; lower profiles). Independent quantification by DRIP-qPCR -/+ RNase H (RNH) treatment (striped bars) is shown in the histogram to the right (n ≥ 4; mean ± SEM normalized to DMSO WT; ns, not significant). *HSPA8* levels decline in WT and KO cells after PMA treatment in a manner that is independent of A3B.

f-g, IF images and quantification of MCF10A (WT) and *A3B*-null (KO) cells treated with PMA for the indicated times and stained with S9.6 (green) and DAPI (blue). Diminution of nucleoplasmic S9.6 signal by exogenous RNase H (RNH) confirmed signal specificity (representative images; 5 μm scale bar; n > 100 nuclei per condition; red bars represent mean ± SEM; **, $P < 0.01$ ****, $P < 0.0001$ by Mann-Whitney test).

Fig. 7. A3B biochemical activities required for R-loop resolution

a, Schematics of the nucleic acids used in biochemical experiments (5' fluorescent label indicated by yellow star). The 15mer short ssDNA and short RNA were used in EMSAs

bioRxiv preprint doi: https://doi.org/10.1101/2021.08.30.458235; this version posted August 31, 2021. The copyright holder for this preprint (which was not certified by peer review) is the author/funder, who has granted bioRxiv a license to display the preprint in perpetuity. It is made available under aCC-BY-NC-ND 4.0 International license.

in panels b and f, and the 62mer long ssDNA was used alone or as annealed to the indicated complementary nucleic acids (black, DNA; red, RNA) in other experiments.

b, Native EMSAs of A3B binding to fluorescently labeled short 15mer ssDNA or RNA in the presence of increasing concentrations of otherwise identical unlabeled competitor. The corresponding quantification shows the average fraction bound to substrate +/- SD from 3 independent experiments.

c, Substrates in panel a tested qualitatively for deamination by A3B. Negative (-) and positive (+) controls are the long ssDNA alone and deaminated by recombinant A3A.

d, A quantitative time course of A3B-catalyzed deamination of the long ssDNA vs an R-loop (short) substrate (mean +/- SD of n = 3 independent experiments are shown with most error bars smaller than the symbols).

e, Subcellular localization of A3B-eGFP (WT), Mut1, and Mut2 in U2OS cells (scale bar = 10 μM).

f, EMSAs comparing A3B WT and Mut2 binding to short 15mer ssDNA and RNA in the presence of increasing concentrations of otherwise identical unlabeled competitor ssDNA or RNA. The corresponding quantification shows the average fraction bound to substrate +/- SD from 3 independent experiments.

g, Quantitative comparison of A3B WT and Mut2 deamination of the long ssDNA versus an R-loop (short) substrate. Representative gels are shown for the time-dependent accumulation of product, along with quantitation of 3 independent experiments (mean +/- SD with most error bars smaller than the symbols; for comparison the WT data are the same as those in panel d).

h, IF images and quantification of U2OS cells expressing the indicated eGFP construct

bioRxiv preprint doi: https://doi.org/10.1101/2021.08.30.458235; this version posted August 31, 2021. The copyright holder for this preprint (which was not certified by peer review) is the author/funder, who has granted bioRxiv a license to display the preprint in perpetuity. It is made available under aCC-BY-NC-ND 4.0 International license.

(green) and stained with S9.6 (red) and DAPI (blue; 5 μm scale bar; n > 60 nuclei per condition; red bars represent mean ± SEM; ****, $P < 0.0001$ by one-way ANOVA; ns, not significant).

Fig. 8. R-Loop mutagenesis and *kataegis* by APOBEC3B

a, Cartoon of a working model for A3B-mediated R-loop resolution with and without associated mutations. Other R-loop regulatory factors are depicted in shades of green and blue. Transcription, splicing, and other RNA- and R-loop-associated complexes are not shown for clarity.

b, A dot plot showing the fraction of APOBEC3-attributed mutations (per Mbp per tumor) in the indicated overexpressed gene groups (FC, fold-change in breast tumors relative to the average observed in normal breast tissues). Pairwise comparisons are significant for all combinations of the lowest 4 versus the highest 3 expression groups ($P < 1 \times 10^{-12}$ by Welsh's t-test).

c, Stacked bar graphs showing the proportion of each COSMIC mutation signature in TCGA breast tumors with mutations in splice factor genes or not (n = 81 splice factor mutated tumors; n = 841 for non-splice factor mutated tumors; $P < 0.017$ by Fisher's exact test). The APOBEC3 signature percentage (red) is comprised of COSMIC signatures 2 and 13, and other signatures are shown in different shades of gray.

d, Quantification of nucleoplasmic R-loop levels in U2OS cells expressing an empty vector (EV) control or A3B following a 2 hr treatment with DMSO or the splicing inhibitor Plad B (n > 50 nuclei per condition; red bars represent mean ± SEM; ****, $P < 0.0001$ by two-tailed unpaired t-test).

bioRxiv preprint doi: https://doi.org/10.1101/2021.08.30.458235; this version posted August 31, 2021. The copyright holder for this preprint (which was not certified by peer review) is the author/funder, who has granted bioRxiv a license to display the preprint in perpetuity. It is made available under aCC-BY-NC-ND 4.0 International license.

e, Distribution of the distances to the nearest SV of all non-clustered APOBEC3 mutations (gold), all *kataegic* mutation events (teal), and R-loop associated APOBEC3 *kataegic* mutations (red).

f-g, Dot plot representations of short (≥3) and long (≥5) APOBEC3 *kataegic* tracts in PCAWG breast tumor WGS. The x- and y-axis reports A3B-associated 5'-RTCA and A3A-associated 5'-YTCA enrichments, respectively. Dashed lines indicate where non-skewed distributions should cluster, red dots represent data from specimens with at least one R-loop-associated *kataegic* event, and the gray ovals highlight the area in which 5'-RTCA enrichments occur (Mann-Whitney U-test *Q*-values indicated in each plot).

h, Representative NTS *kataegic* events in the indicated genes. Wild-type trinucleotides and mutational outcomes are indicated.

a

			A3B AP-MS			S9.6 AP-MS		
			Percent	Peptides ID'd		Percent	Peptides ID'd	
Protein Name	kDa	Accession	Coverage	Unique	Total	Coverage	Unique	Total
APOBEC3B	46	Q9UH17	59.7	21	119	11.5	5	5
RBM8A	20	Q9Y5S9	40.2	6	20	31.0	4	4
SRSF10	31	O75494	31.7	9	28	24.0	9	9
MAP4	121	P27816	31.6	26	35	7.20	6	6
SF3B2	100	Q13435	30.8	27	47	10.5	8	8
HNRNPUL1	96	Q9BUJ2	30.5	31	79	21.4	16	16
SRSF7	27	Q16629	29.4	9	23	35.3	9	10
SNRNP200	244	O75643	24.1	40	51	17.9	30	30
MMTAG2	29	Q9BU76	24.0	5	11	34.6	7	7
RCC2	56	Q9P258	23.0	11	19	13.0	6	6
HNRNPH2	49	P55795	22.3	9	35	36.7	5	13
SKIV2L2	118	P42285	22.2	23	52	9.60	8	8
ZFR	117	Q96KR1	18.3	13	30	34.6	25	25
SAFB	103	Q15424	14.8	11	31	32.3	15	29
MOV10	114	Q9HCE1	11.2	11	19	29.6	22	22

b

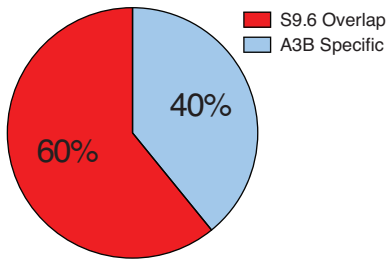

c

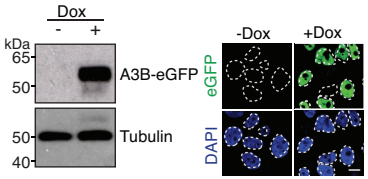

d

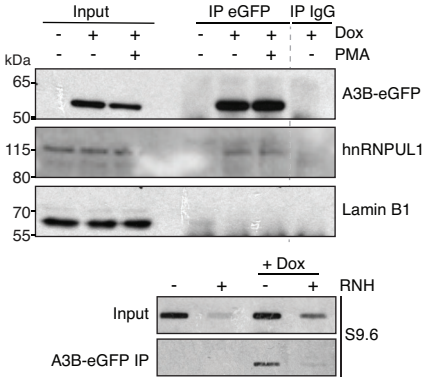

e

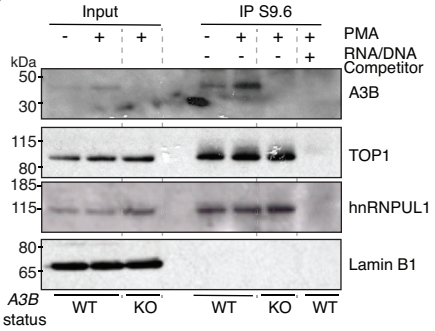

Figure 1

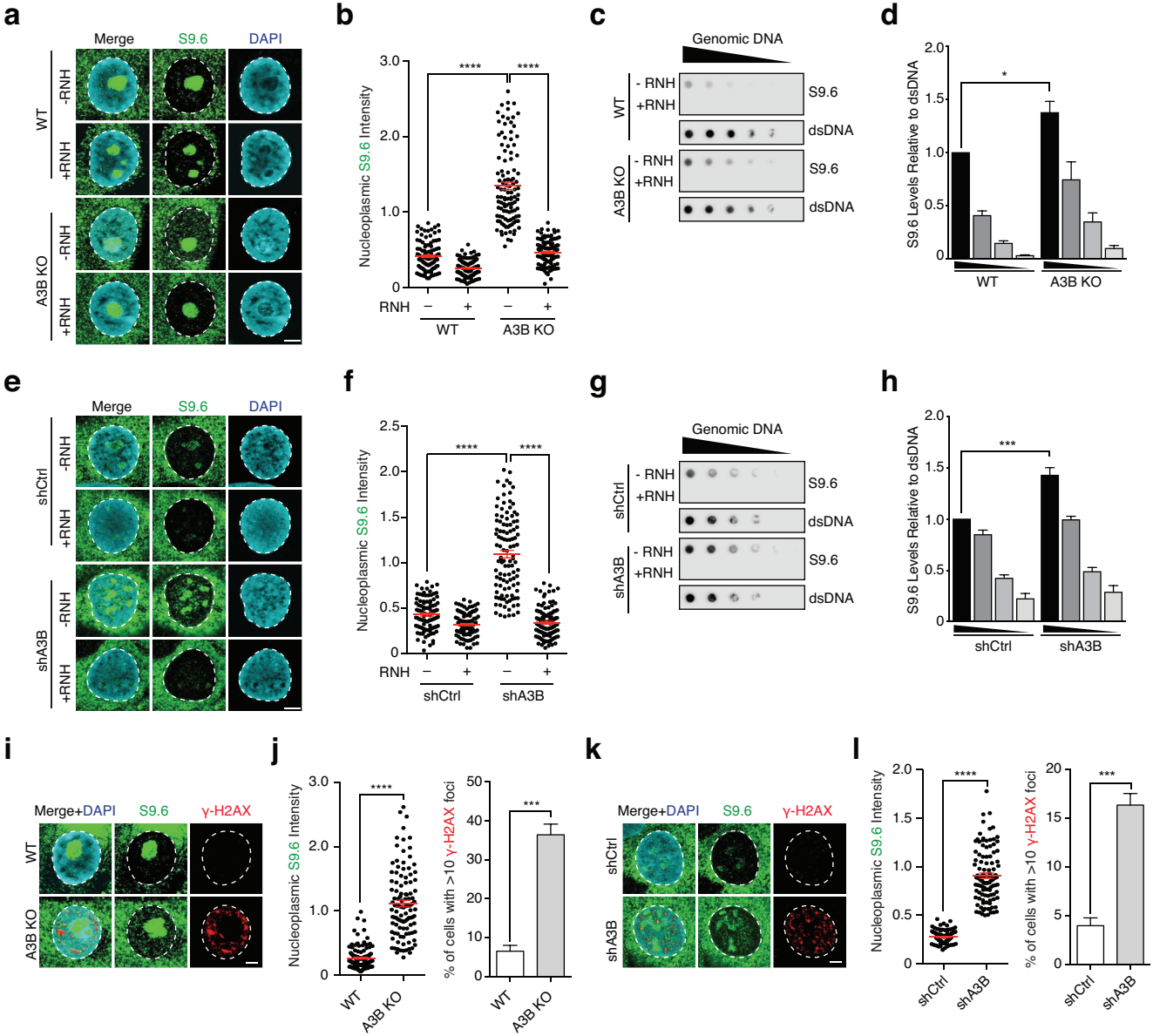
a
Merge
S9.6
DAPI
WT
-RNH
+RNH
A3B KO
-RNH
+RNH
b
Nucleoplasmic S9.6 Intensity
****
****
RNH
WT
A3B KO
c
Genomic DNA
WT
- RNH
+RNH
S9.6
dsDNA
A3B KO
- RNH
+RNH
S9.6
dsDNA
d
S9.6 Levels Relative to dsDNA
*
WT
A3B KO
e
Merge
S9.6
DAPI
shCtrl
-RNH
+RNH
shA3B
-RNH
+RNH
f
Nucleoplasmic S9.6 Intensity
****
****
RNH
shCtrl
shA3B
g
Genomic DNA
shCtrl
- RNH
+RNH
S9.6
dsDNA
shA3B
- RNH
+RNH
S9.6
dsDNA
h
S9.6 Levels Relative to dsDNA
***
shCtrl
shA3B
i
Merge+DAPI
S9.6
γ-H2AX
WT
A3B KO
j
Nucleoplasmic S9.6 Intensity
****
% of cells with >10 γ-H2AX foci
***
WT
A3B KO
k
Merge+DAPI
S9.6
γ-H2AX
shCtrl
shA3B
l
Nucleoplasmic S9.6 Intensity
****
% of cells with >10 γ-H2AX foci
***
shCtrl
shA3B

Figure 2

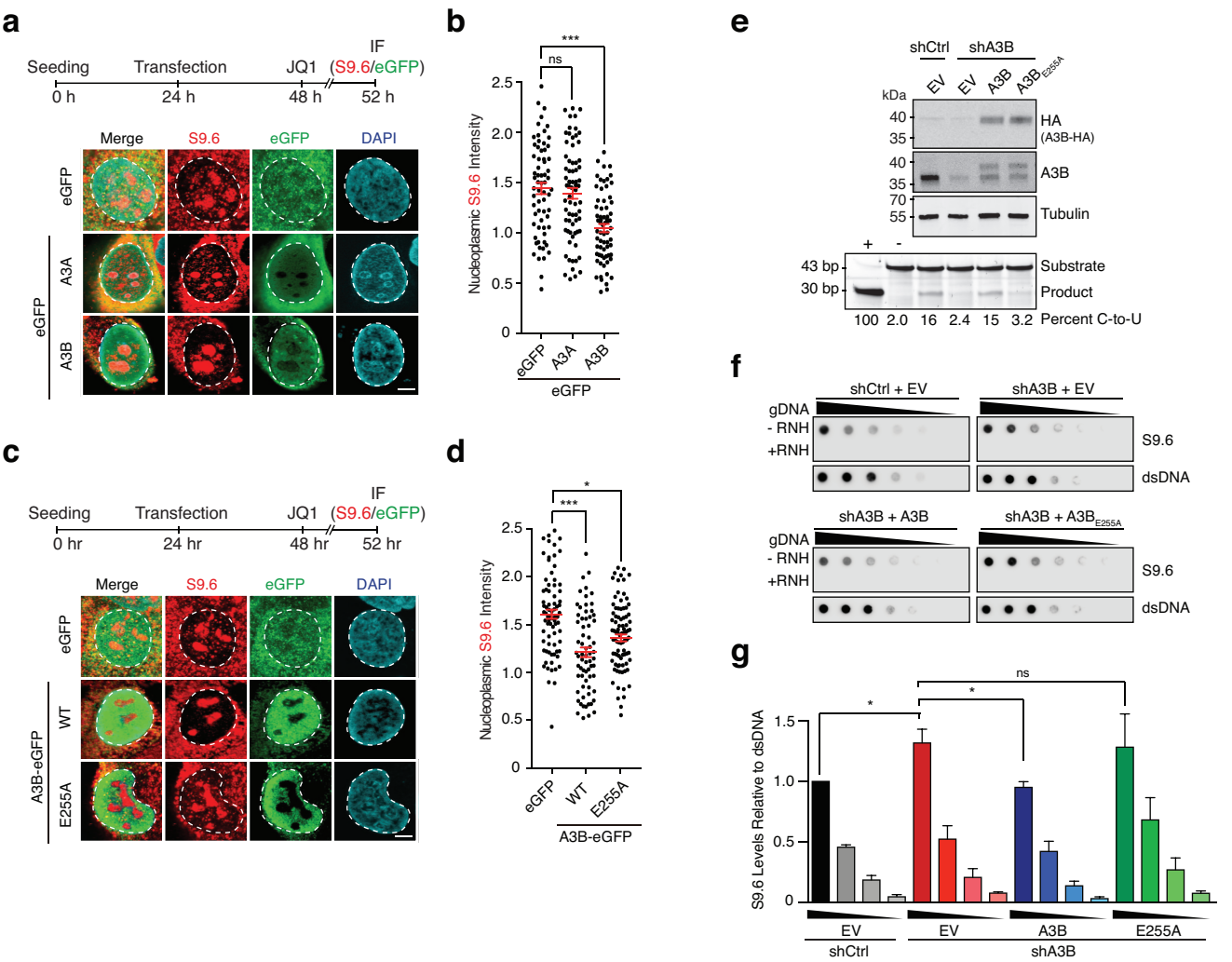
a
Seeding
Transfection
JQ1
IF (S9.6/eGFP)
0 h
24 h
48 h
52 h
Merge
S9.6
eGFP
DAPI
eGFP
A3A
A3B
b
ns
***
Nucleoplasmic S9.6 Intensity
eGFP
A3A
A3B
c
Seeding
Transfection
JQ1
IF (S9.6/eGFP)
0 hr
24 hr
48 hr
52 hr
WT
E255A
A3B-eGFP
d
*
***
e
shCtrl
shA3B
EV
A3B
A3B E255A
kDa
HA (A3B-HA)
Tubulin
43 bp
30 bp
Substrate
Product
Percent C-to-U
100 2.0 16 2.4 15 3.2
f
shCtrl + EV
shA3B + EV
shA3B + A3B
shA3B + A3B E255A
gDNA
- RNH
+RNH
S9.6
dsDNA
g
ns
S9.6 Levels Relative to dsDNA
shCtrl
shA3B

Figure 3

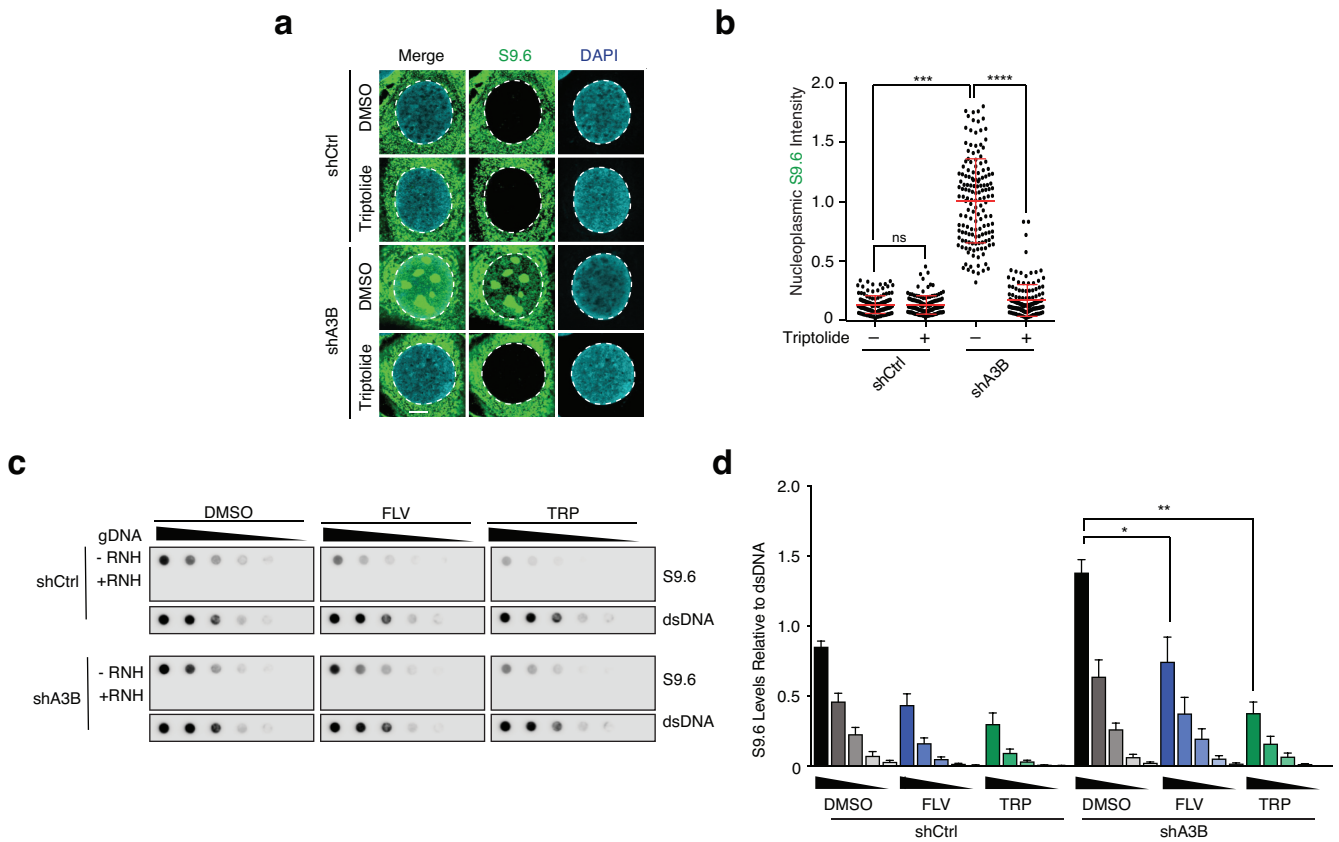
a
Merge
S9.6
DAPI
shCtrl
shA3B
DMSO
Triptolide
b
Nucleoplasmic S9.6 Intensity
2.0
1.5
1.0
0.5
0
***
****
ns
Triptolide
–
+
shCtrl
shA3B
c
DMSO
FLV
TRP
gDNA
shCtrl
- RNH
+RNH
shA3B
S9.6
dsDNA
d
S9.6 Levels Relative to dsDNA
2.0
1.5
1.0
0.5
0
**
*
DMSO
FLV
TRP
shCtrl
shA3B

Figure 4

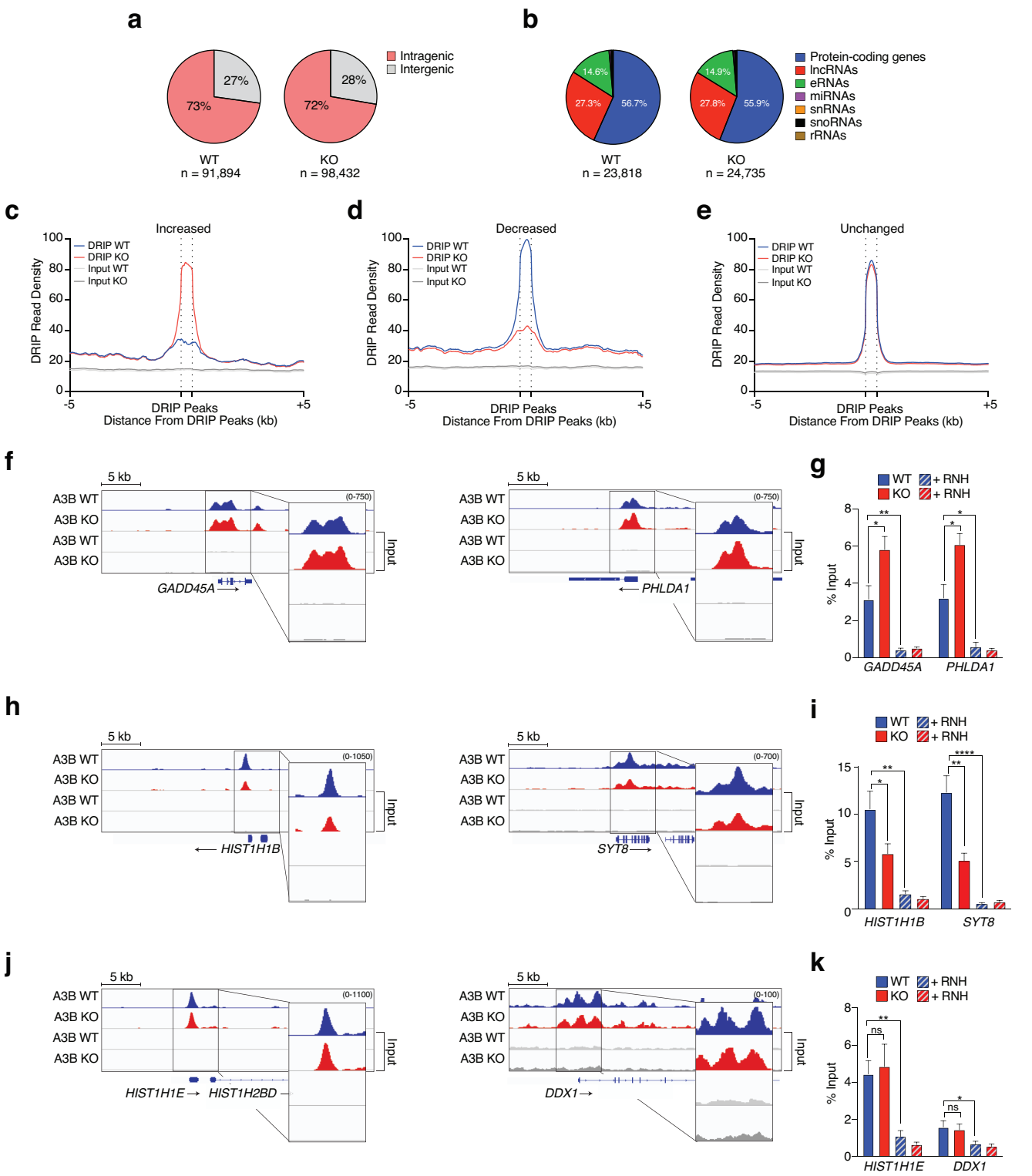
a
Intragenic
Intergenic
27%
73%
28%
72%
WT
n = 91,894
KO
n = 98,432
b
Protein-coding genes
lncRNAs
eRNAs
miRNAs
snRNAs
snoRNAs
rRNAs
14.6%
27.3%
56.7%
14.9%
27.8%
55.9%
WT
n = 23,818
KO
n = 24,735
c
Increased
d
Decreased
e
Unchanged
DRIP WT
DRIP KO
Input WT
Input KO
DRIP Read Density
DRIP Peaks
Distance From DRIP Peaks (kb)
f
5 kb
A3B WT
A3B KO
Input
GADD45A
PHLDA1
g
% Input
WT
KO
+ RNH
h
HIST1H1B
SYT8
i
j
HIST1H1E
HIST1H2BD
DDX1
k
ns

Figure 5

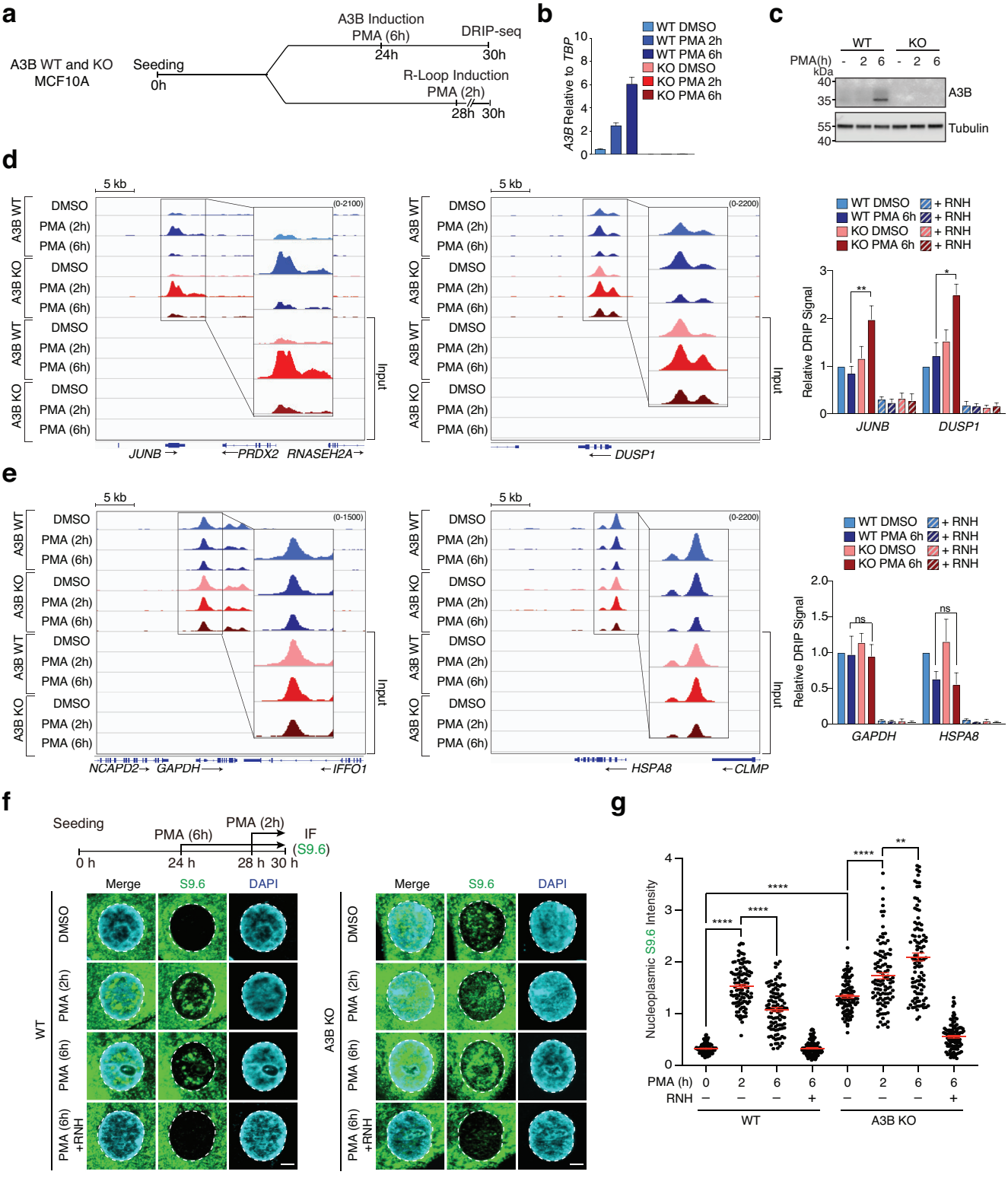
a
A3B WT and KO MCF10A
Seeding 0h
A3B Induction PMA (6h) 24h
DRIP-seq 30h
R-Loop Induction PMA (2h) 28h 30h
b
A3B Relative to TBP
WT DMSO
WT PMA 2h
WT PMA 6h
KO DMSO
KO PMA 2h
KO PMA 6h
c
WT KO
PMA(h) - 2 6 - 2 6
kDa
A3B
Tubulin
d
5 kb
A3B WT
A3B KO
DMSO
PMA (2h)
PMA (6h)
Input
JUNB PRDX2 RNASEH2A
DUSP1
WT DMSO + RNH
WT PMA 6h + RNH
KO DMSO + RNH
KO PMA 6h + RNH
Relative DRIP Signal
e
NCAPD2 GAPDH IFFO1
HSPA8 CLMP
ns
f
Seeding
PMA (6h)
PMA (2h)
IF (S9.6)
0 h 24 h 28 h 30 h
Merge S9.6 DAPI
WT
A3B KO
PMA (6h) +RNH
g
Nucleoplasmic S9.6 Intensity
PMA (h) 0 2 6 6 0 2 6 6
RNH – – – + – – – +
WT
A3B KO

Figure 6

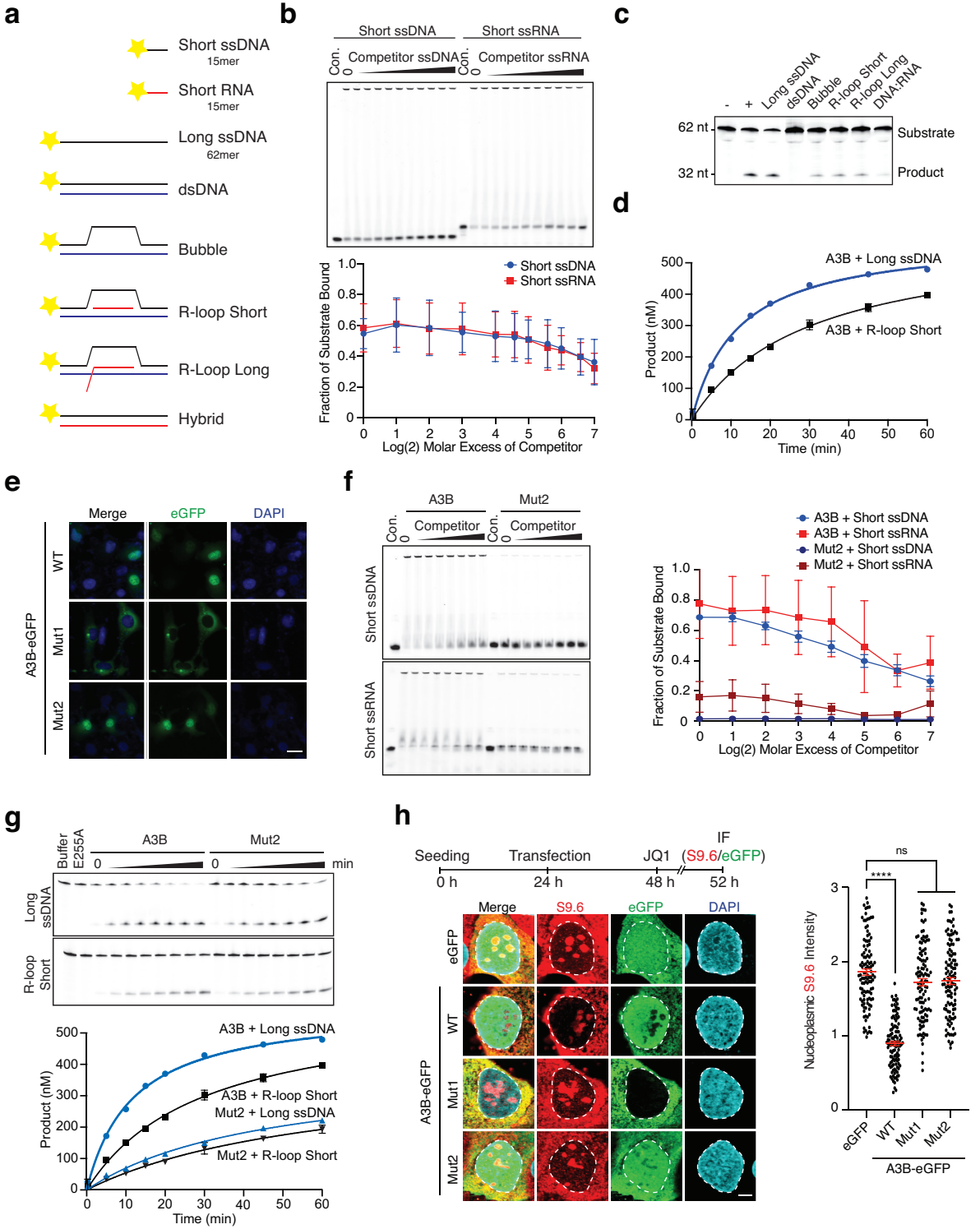
a
Short ssDNA
15mer
Short RNA
15mer
Long ssDNA
62mer
dsDNA
Bubble
R-loop Short
R-Loop Long
Hybrid
b
Short ssDNA
Short ssRNA
Con.
0
Competitor ssDNA
Competitor ssRNA
Fraction of Substrate Bound
Log(2) Molar Excess of Competitor
c
Long ssDNA
dsDNA
Bubble
R-loop Short
R-loop Long
DNA:RNA
62 nt
32 nt
Substrate
Product
d
A3B + Long ssDNA
A3B + R-loop Short
Product (nM)
Time (min)
e
Merge
eGFP
DAPI
A3B-eGFP
WT
Mut1
Mut2
f
A3B
Mut2
Competitor
Short ssDNA
Short ssRNA
A3B + Short ssDNA
A3B + Short ssRNA
Mut2 + Short ssDNA
Mut2 + Short ssRNA
Fraction of Substrate Bound
Log(2) Molar Excess of Competitor
g
Buffer
E255A
A3B
Mut2
min
Long ssDNA
R-loop Short
A3B + Long ssDNA
A3B + R-loop Short
Mut2 + Long ssDNA
Mut2 + R-loop Short
Product (nM)
Time (min)
h
Seeding
Transfection
JQ1
IF (S9.6/eGFP)
0 h
24 h
48 h
52 h
Merge
S9.6
eGFP
DAPI
A3B-eGFP
WT
Mut1
Mut2
ns
****
Nucleoplasmic S9.6 Intensity

Figure 7

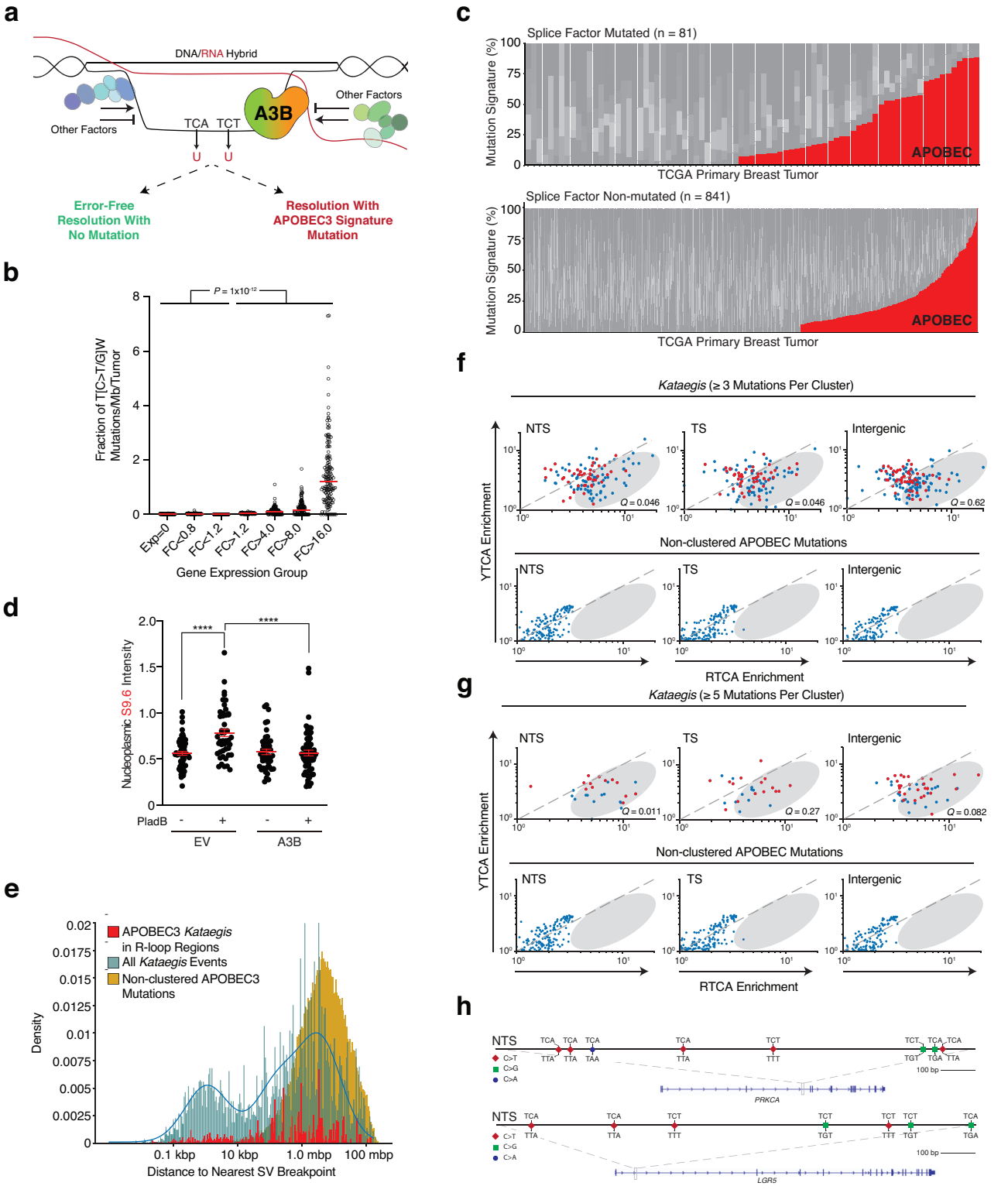
a
DNA/RNA Hybrid
Other Factors
A3B
Other Factors
TCA TCT
U U
Error-Free Resolution With No Mutation
Resolution With APOBEC3 Signature Mutation
b
P = 1x10-12
Fraction of T[C>T/G]W Mutations/Mb/Tumor
Exp=0
FC<0.8
FC<1.2
FC>1.2
FC>4.0
FC>8.0
FC>16.0
Gene Expression Group
c
Splice Factor Mutated (n = 81)
Mutation Signature (%)
APOBEC
TCGA Primary Breast Tumor
Splice Factor Non-mutated (n = 841)
Mutation Signature (%)
APOBEC
TCGA Primary Breast Tumor
d
Nucleoplasmic S9.6 Intensity
****
****
PladB
EV
A3B
e
APOBEC3 Kataegis in R-loop Regions
All Kataegis Events
Non-clustered APOBEC3 Mutations
Density
0.1 kbp
10 kbp
1.0 mbp
100 mbp
Distance to Nearest SV Breakpoint
f
Kataegis (≥ 3 Mutations Per Cluster)
NTS
TS
Intergenic
YTCA Enrichment
Q = 0.046
Q = 0.046
Q = 0.62
Non-clustered APOBEC Mutations
RTCA Enrichment
g
Kataegis (≥ 5 Mutations Per Cluster)
NTS
TS
Intergenic
YTCA Enrichment
Q = 0.011
Q = 0.27
Q = 0.082
Non-clustered APOBEC Mutations
RTCA Enrichment
h
NTS
C>T
C>G
C>A
100 bp
PRKCA
LGR5

Figure 8